AD-A083 940 BUSINESS AND TECHNOLOGICAL SYSTEMS INC SEABROOK MD F/G 13/10
PROGRAM DEVELOPMENT TO STUDY FAIRED TOWLINES.(U)
FEB 80 J B EADES, V MAJER N00014-78-C-0410
UNCLASSIFIED BTS-IR-80-102 ONR-CR298-003-2F NL

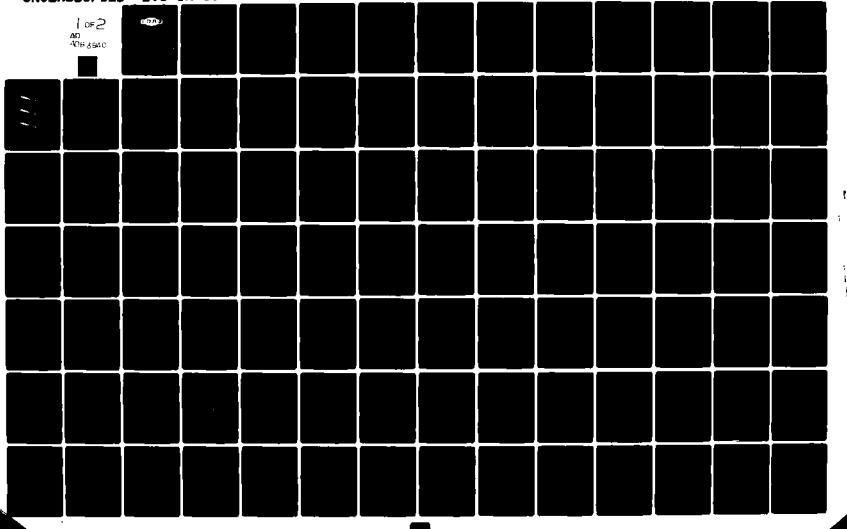

ONR CR298-003-2F

PROGRAM DEVELOPMENT TO STUDY FAIRED TOWLINES

J. B. Eades, Jr.

V. Majer

BUSINESS AND TECHNOLOGICAL SYSTEMS, INC.
Seabrook, Maryland 20801

Contract No. N00014-78-C-0410

February 1980

FINAL REPORT FOR PERIOD 1 MAY 1979 - 29 FEBRUARY 1980

PREPARED FOR THE
OFFICE OF NAVAL RESEARCH • 800 N. QUINCY ST. • ARLINGTON, VA. 22217

Change of Address

Organizations receiving reports on the initial distribution list should confirm correct address. This list is located at the end of the report. Any change of address or distribution should be conveyed to the Office of Naval Research, Code 211, Arlington, VA 22217.

Disposition

When this report is no longer needed, it may be transmitted to other organizations. Do not return it to the originator or the monitoring office.

Disclaimer

The findings and conclusions contained in this report are not to be construed as an official Department of Defense or Military Department position unless so designated by other official documents.

Reproduction

Reproduction in whole or in part is permitted for any purpose of the United States Government.

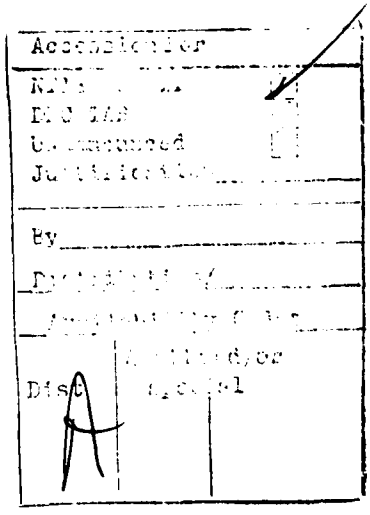

UNCLASSIFIED

SECURITY CLASSIFICATION OF THIS PAGE *(When Data Entered)*

(19) REPORT DOCUMENTATION PAGE

READ INSTRUCTIONS BEFORE COMPLETING FORM

(18) 1. REPORT NUMBER: ONR CR298-003-2F	2. GOVT ACCESSION NO.: AD-A083 944
3. RECIPIENT'S CATALOG NUMBER:	
(6) 4. TITLE (and Subtitle): PROGRAM DEVELOPMENT TO STUDY FAIRED TOWLINES,	(9) 5. TYPE OF REPORT & PERIOD COVERED: Final Report, 1 MAY 1979 — 29 FEB 1980
6. PERFORMING ORG. REPORT NUMBER: BTS-IR-80-102 (14)	
(10) 7. AUTHOR(s): J. B. Eades, Jr. and V. Majer	(15) 8. CONTRACT OR GRANT NUMBER(s): N00014-78-C-0410
9. PERFORMING ORGANIZATION NAME AND ADDRESS: Business and Technological Systems, Inc. 10210 Greenbelt Road, Suite 440 Seabrook, Maryland 20801	10. PROGRAM ELEMENT, PROJECT, TASK AREA & WORK UNIT NUMBERS: 61153N RR023-01-83, 1-12 NR 298-003
11. CONTROLLING OFFICE NAME AND ADDRESS: Office of Naval Research, Code 211 800 North Quincy Street Arlington, Virginia 22217 (11)	12. REPORT DATE: February 1980
	13. NUMBER OF PAGES: 103
14. MONITORING AGENCY NAME & ADDRESS *(if different from Controlling Office)* (12) 102	15. SECURITY CLASS. *(of this report)*: Unclassified
	15a. DECLASSIFICATION/DOWNGRADING SCHEDULE

16. DISTRIBUTION STATEMENT *(of this Report)*

Approved for public release, distribution unlimited

(16) KKP230 1

17. DISTRIBUTION STATEMENT *(of the abstract entered in Block 20, if different from Report)*

(17) KKP230 183

18. SUPPLEMENTARY NOTES

19. KEY WORDS *(Continue on reverse side if necessary and identify by block number)*

Towlines, faired towlines, faired towing cables, kiting, airfoils, airfoil chordwise deflection, pressure distribution, hydrodynamic/structural response, computer program, hydrodynamic/structural response computational program.

20. ABSTRACT *(Continue on reverse side if necessary and identify by block number)*

Various computational algorithms have been developed for use in the design and analysis of integrated faired towlines. In the first phase of this development a computer program (HYDROSAP) was constructed. This system determined the two-dimensional response of a flexible streamlined profile section, to its hydrodynamic loading, under simulated towing conditions. The second phase of the development has provided algorithms which, first, determine the section's mechanical characteristics (areas, →

DD FORM 1 JAN 73 1473 EDITION OF 1 NOV 65 IS OBSOLETE S/N 0102-014-6601

390 922

SECURITY CLASSIFICATION OF THIS PAGE *(When Data Entered)*

torsion and shear centers, inertia coefficients, etc.) and, second, examines the dynamic behavior of a faired towline under quasi steady towing conditions.

Since these cables have varied and discontinuous elastic properties, all of the structural programs are constructed using the finite element technique. This provides a convenient means to accomodate the variety of conditions which are present in a problem situation.

The presently developed three-dimensional cable program does not have the full capability intended for this analysis tool. A full elastic response of the system has not been modelled in the existing system. The two-dimensional program, however, is a complete and operating system as is the several supporting algorithms used in defining the sectional mechanical properties for an integrated, faired cable system.

TABLE OF CONTENTS

TABLE OF CONTENTS (cont'd.)

LIST OF TABLES

LIST OF FIGURES

LIST OF FIGURES (cont'd.)

1.0 INTRODUCTION

In support of the Navy's continuing program to develop high speed towed-body systems, this report describes the extension of an earlier analysis capabilities programming effort. It is the results from this most recent work which we are reporting here.

To provide some background for the present tasks, a brief review of our previous efforts is given below.

The initial work was undertaken to provide an analysis and numerical demonstration capability for the study of streamlined fairings. These fairings are to be used in high speed underwater towing situations. The construction of the fairings is such that streamwise distortions are able to occur; and, that a likely consequence from them would be some "undesirable behavior" from the towline. What was not anticipated, but what has actually occured, was an uncontrolled "kiting" of these tow cables -- leading to unacceptable towing performance.

Since the physics of this problem was not immediately apparent, and the remedial measures taken to correct the adverse happenings did not resolve the situation; it was proposed that some numerical analysis tools be developed to aid in the study and understanding of these situations. A first step in this effort was the development of the computational algorithm which we have labled HYDROSAP. This program seeks to describe the physical deformations produced on a typical streamlined, flexible, two-dimensional fairing section as a consequence of the hydrodynamic loads impressed on it. The loadings which these airfoil-type sections are subjected to are those typical to any streamlined (two-dimensional) shape operating at an angle of attack in a steady, viscous fluid flow. Because these fairings <u>are</u> flexible -- their after-sections are constructed from a rubber-like material -- the chordwise distortions cause the flow field to be altered; which, in turn, produces other chordwise distortions; which, in turn, changes the flow pattern, ••• etc.

As a consequence of these actions it is apparent that the mathematical modelling of this phenomenon requires an iterative method of solution. A solution which (first) determines the hydrodynamic "loads" on the profile section; then ascertains the distortions due to this loading; subsequently, redefining the loads on the (deformed) profile; and so on. (Incidentally, this methodology is depicted, schematically, on Figure 2.1 in the next section of this report.)

Being cognizant of the fact the HYDROSAP treats only the two-dimensional problems; that it will merely "point" to the probable causes of kiting; then, a next logical step (in the developmental process) was that of modelling the three-dimensional problem and seeking a more likely and realistic answer to the real-world situation.

The three-dimensional, computational program development is basically what is being reported on here. However, it should be noted that we have only begun the task of developing a three-dimensional, numerical analysis tool. In this report we will describe the current status of these efforts; outline what has been accomplished; discuss the findings and results from this work; and describe those things which we believe are needed to accomplish the goals for this overall task. These goals, incidentally, will only be realized when a full, three-dimensional analysis program has been developed; and after it has been checked and verified against experimental evidence. Then, and only then, can this work be said to be "complete".

In this second stage of the development effort two primary computational algorithms have been developed. One, given the acronym SHCENT, is used to describe the mechanical-structural characteristics of the cable's cross-sections. Its principal outputs are the shear-center location and torsional rigidity; both of which depend on the shape and the material description of the cross-sections. In addition, certain other parameters (elastic and geometric properties) needed in the structural analysis are also computed here.

With the loading information provided from HYDROSAP, and the cross-sectional mechanical properties obtained from SHCENT, the second computational program, TOWLINE, is used to ascertain the three-dimensional dynamic response of the cable. This algorithm was developed using a finite element method technique. The cable's elements were build around a standard beam model, one which is assumed to suffer large displacements but have only small strains.

The TOWLINE program, in its present state of development, is described in this document. It should be recognized that the existing version of TOWLINE is not ready to be used on a production basis, even though it has been used in an exploratory fashion on several "model" cable problems as we describe in Section 3.0, below. The original intent of this developmental task was to provide the existing computational framework; to enhance it during subsequent efforts; and, to perfect the model through a verification with experimental data and evidence.

In the following sections of this document we will (first) outline our previous developments (HYDROSAP); then, we will describe, discuss and comment on the achievements and results obtained in the current task effort.

2.0 TWO-DIMENSIONAL FLOW-STRUCTURE INTERACTION

2.1 Overview of the Two-Dimensional Problem

A study of the nonlinear interactions between hydrodynamic and structural effects, on a flexible two-dimensional streamlined cross-section when exposed to a steady, viscous fluid flow, was a first step in the analysis of faired towing cable systems. The resulting cross-section's deformed shape alters the cable's local hydrodynamic characteristics and, consequently, affects its global behavior. This build-up in interaction of structural and hydrodynamic effects is pictured schematically in Figure 2.1.

In our iterative approach to this problem we determine a pressure distribution corresponding to the base (or design) profile shape. This streamlined section is assumed to be at a fixed angle of attack, α, relative to the free stream velocity vector, V. This (base) pressure distribution is then applied to a suitably described finite element model of the fairing to determine a structurally "deformed" profile. This altered shape, in turn, develops an altered pressure distribution -- which in turn deforms the profile -- which in turn ••• etc. This process continues, in an iterative fashion, until the incremental change in structural deformation is "sufficiently small" to describe the converged (deformed) profile and its attendant pressure distribution. Typically a converged solution is achieved after some five to ten iterations.

The HYDROSAP computer program is a mechanization of the process described above. HYDROSAP is based on various elements of two existing computer programs; the NASA Multicomponent Two-dimensional Viscous Airfoil Program (referred to as HYDRO in the sequel) and the University of California's Non-linear Structural Analysis Program (NONSAP). The various program elements, plus the many components developed for our programs's mechanizations, were integrated into a single software system.

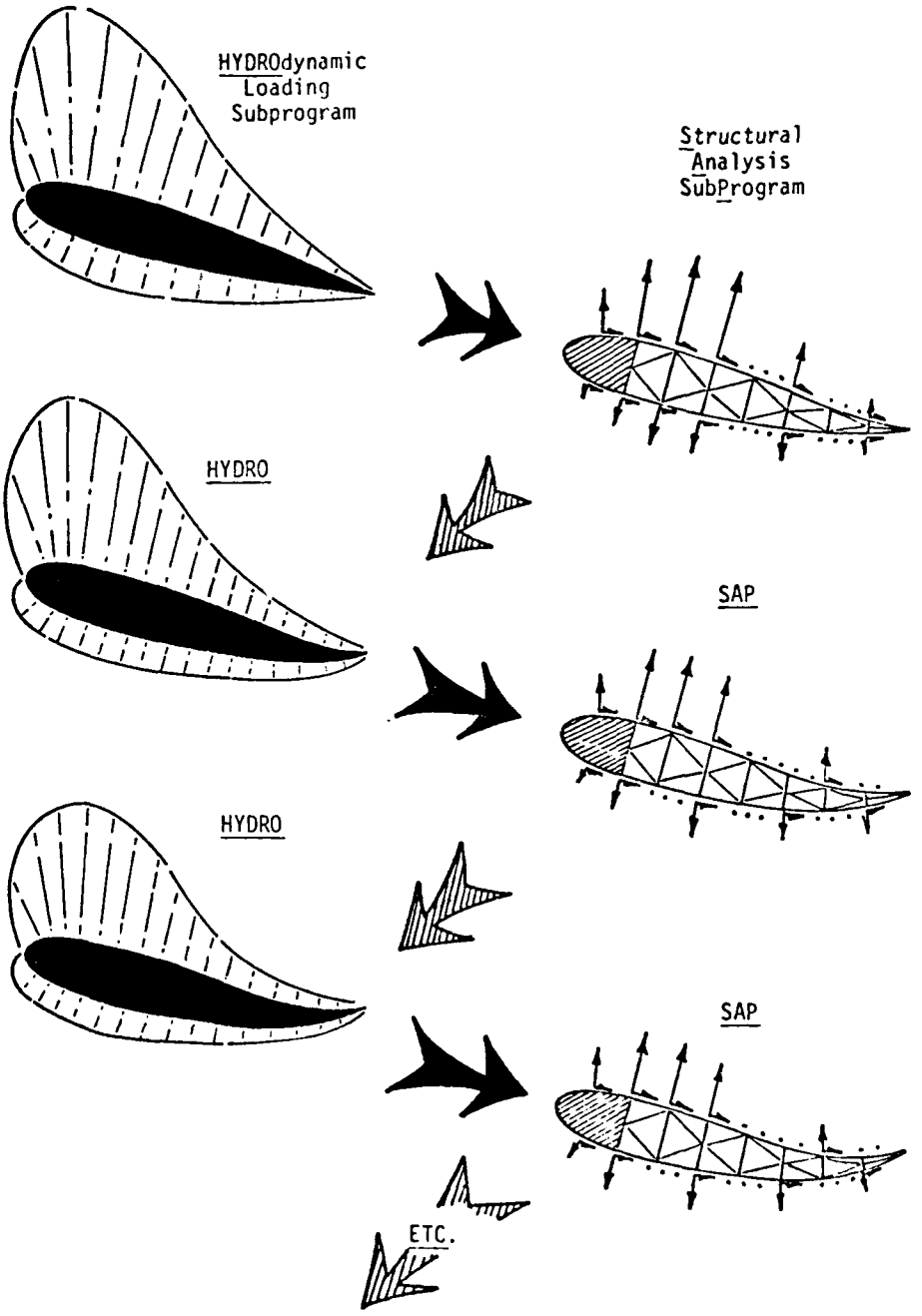

Figure 2.1
A Schematic Depicting the Iterative Operations of HYDROSAP --
A Hydrodynamic Loading, Structural Response Software System

In sections 2.2.1 and, respectively, 2.2.2 below, we will briefly describe these solution algorithms. A more detailed discussion, including a description of program input and operating requirements, can be found in the HYDROSAP documentation [1].[1]

That report also describes, in full detail, the several features of the HYDROSAP system. In particular, a description of the BTS-developed executive, DRIVER, and other features which would be of interest, primarily, to the software user, appear therein.

2.2 Solution Algorithms

2.2.1 The Fluid Flow Field

Given a pointwise shape description of a two-dimensional profile, the HYDRO routines compute the velocity destribution, over the profile's surface, by a superposition of velocity fields. These are the primary velocity distributions due to thickness and to profile camber. This is a potential flow solution, one which must be modified to account for viscous (boundary layer) effects by one of two methods: (1) a modifying of the profile's geometry; or, (2) introducing a distribution of source singularities to account for the boundary layer thickness distribution. The potential flow field (thickness and camber effects) is then re-computed, taking into account the boundary layer displacement thickness over the profile. This process reoccurs, iteratively, until changes in the velocity field fall below some pre-set tolerance. Of course, if the viscous boundary layer is neglected, the computations are not iteratively sequenced and the corresponding run time is considerably shortened.

Calculations for the velocity fields, due to thickness and camber, make use of Oellers' Vortex Distribution Method [5], using the scheme which is outlined in [2] and [3]. Incorporated into these computations is a procedure to satisfy the Kutta condition for the profile. The procedure represents a modified Kutta condition wherein the upper and lower

[1]Numerals in brackets [ ] denote the reference numbers in Section 5.0.

surface vortex strengths are matched, in magnitude, but assigned opposing signs at the foil's downstream terminus.

If the viscous boundary layer is to be simulated by a distribution of source singularities then subroutine SOURCE is called. Otherwise the boundary layer's influence is provided for by modifying the velocity field for camber effects. For those cases where the foil's trailing edge thickness is not zero, the velocity field due to thickness is altered through a closure of the geometry one chord length downstream of the true trailing edge.

The present version of HYDRO does not compute flow separation, although recent work in this area could be incorporated [6]. Also, the drag increment due to the wake behind the foil is based solely on empirical results from tests on truncated profiles.

The laminar boundary layer computations in HYDRO are based on Goradia's adaptation of the work by Cohen and Reshotko [7], and on Schlichting [8]. In addition to computing the laminar boundary layer thickness, the program determines the laminar friction coefficients and predicts boundary layer transition points. Truckenbrodt's integral method [9] is used to compute parameters describing the turbulent boundary layer.

Finally, the usual force and moment coefficients for the profile are computed from the pressure and shear force distributions. The moment coefficients -- at both the quarter-chord point and at the leading edge -- are determined. In addition to the "usual" drag coefficient, the drag coefficient based on the approximate theory of Squire and Young [10] is calculated and displayed in the output.

2.2.2 A Cross-Section's Mechanical Response

Given a description of the profile's topology, the mechanical properties of its constituent materials, and the pressure loading (from HYDRO), NONSAP is used to compute the profile's mechanical response. (The finite element program NONSAP (NONlinear Structural Analysis Program) was originally developed in 1974 [12]). Even though NONSAP may be used to analyze the static or dynamic response of one-, two-, or three-dimensional structures, including the effects of geometric and/or material nonlinearities, we restrict ourselves to its two-dimensional capabilities.

In this section we give a brief overview of NONSAP's capabilities and its operation. However, for a more complete and detailed description of the NONSAP theory and operation, the reader is referred to the original program documentation [11, 12] and to the HYDROSAP documentation [1].

2.2.2.1 Program Description

The NONSAP program was developed to solve static or dynamic, linear or nonlinear structural problems. The allowable nonlinearities may be due to either material behavior (elastic, hyperelastic, and hypoelastic material models are available) or to the effects of large displacements and large strains. The equations of motion from continuum mechanics,governing the behavior of the structure under study, are discretized, in space variables, through the use of isoparametric finite elements. The equations are discretized in the time variable through either a Wilson-Theta or a Newmark-Beta time integration scheme. The resulting nonlinear equations are solved using an incremental method which corresponds to a modified Newton iteration.

The structural systems to be analyzed may be modeled using a variety of finite element types. These are:

- one-dimensional truss elements,
- two-dimensional plane stress or plane strain elements,
- two-dimensional axi-symmetric shell elements, and
- three-dimensional solid or thick shell elements.

Since nonlinearities may be due to nonlinear material behavior as well as to large displacements, or large strains, there are several material descriptions available in the program. These include:

- an isotropic linear elastic material model,
- an orthotropic linear elastic material model,
- the Mooney-Rivlin model,
- an elastic-plastic material with von Mises or Drucker-Prager yield conditions,
- a variable tangent model, and
- a curve description model.

Currently, the *HYDROSAP program makes use only* of the one-dimensional truss finite element, the two-dimensional plane strain element, and the isotropic linear elastic material model. All nonlinearities are, therefore, geometric. Moreover, HYDROSAP uses NONSAP routines in the nonlinear static solution mode with the "updated Lagrangian" solution procedure. As a consequence of the constraints, the discussions below will be restricted to those NONSAP procedures and options which are currently employed in HYDROSAP.

2.2.2.2 Incremental Equilibrium Equations for Structural Systems

Using the well-known and well documented [12, 13] method of finite elements, the incremental nodal point equilibrium equations for an assemblage of finite elements take the form,

$$M\,\ddot{u}(t+\Delta t) + C\,\dot{u}(t+\Delta t) + K(t)\,\Delta u = R(t+\Delta t) - F(t), \qquad (2.1)$$

where

M = the constant mass matrix,
C = the constant damping matrix,
$K(t)$ = the tangent stiffness matrix, described at time t,
$R(t)$ = the external applied load vector, described at time t,
$F(t)$ = the nodal point force vector (of stress-equivalent internal reactions), for time t,
$u(t)$ = the vector of nodal point displacements, at time t,
Δu = the vector of nodal point displacement increments, from time t to time $t+\Delta t$: thus, $u(t+\Delta t) - u(t)$,
t = time, and
Δt = time increment.

Of course, in a static analysis $M=C=0$, while time is regarded only as a loading parameter used for applying the external load in "quasistatic" load increments. Also, in nonlinear analysis, the solution of (2.1) yields only approximate solution increments, Δu. In order to improve the solution accuracy and to prevent the buildup of solution instabilities, equilibrium iterations may be used at selected time steps.

In the nonlinear static case an equation system of the form

$$K(t)(\Delta u)_{i+1} = R(t+\Delta t) - F_i \quad (i=0,1,2,\cdots) \qquad (2.2)$$

is solved by iteration. Here $F_0 = F(t)$ and F_i is the vector of stress-equivalent internal reactions corresponding to the displacement vector $u_i(t+\Delta t) = u_{i-1}(t+\Delta t) + (\Delta u)_i$. The solution of (2.2), by iteration, is clearly a modified Newton method for (2.1).

2.2.2.3 NONSAP Solution Process

The complete NONSAP solution process consists of three distinct stages: input, assembly, and step-by-step solution (See Figure 2.2).

Input Stage

In this stage, control and nodal point input are read and/or generated by the program; and equation numbers for the active degrees of freedom at each nodal point are established. In addition, externally applied load vectors are established and stored on tape. Finally, when the element data are ready and/or generated, element connectivity arrays are established, and all element data are stored on tape.

Assembly Stage

Here the linear and effective linear structural stiffness matrices are assembled and stored on tape, as are the mass and damping matrices (for a dynamic analysis). Matrices are stored in compacted form as one-dimensional arrays. Only the elements below the "skyline" of a matrix are processed, thereby reducing storage, input/output, and computational costs.

Solution Stage

In nonlinear static analysis (the solution mode for which NONSAP routines are used by HYDROSAP) damping and mass effects are neglected. Time serves as a loading parameter only, and the input time step determines the load increment to be applied to the structure during each solution step. The linear stiffness matrix, which was previously assembled and stored on tape, is updated at each solution step. This is accomplished by updating the stiffness matrices, of the nonlinear elements, to form a current tangent stiffness matrix. The load step interval at which this update occurs is one of the NONSAP control inputs.

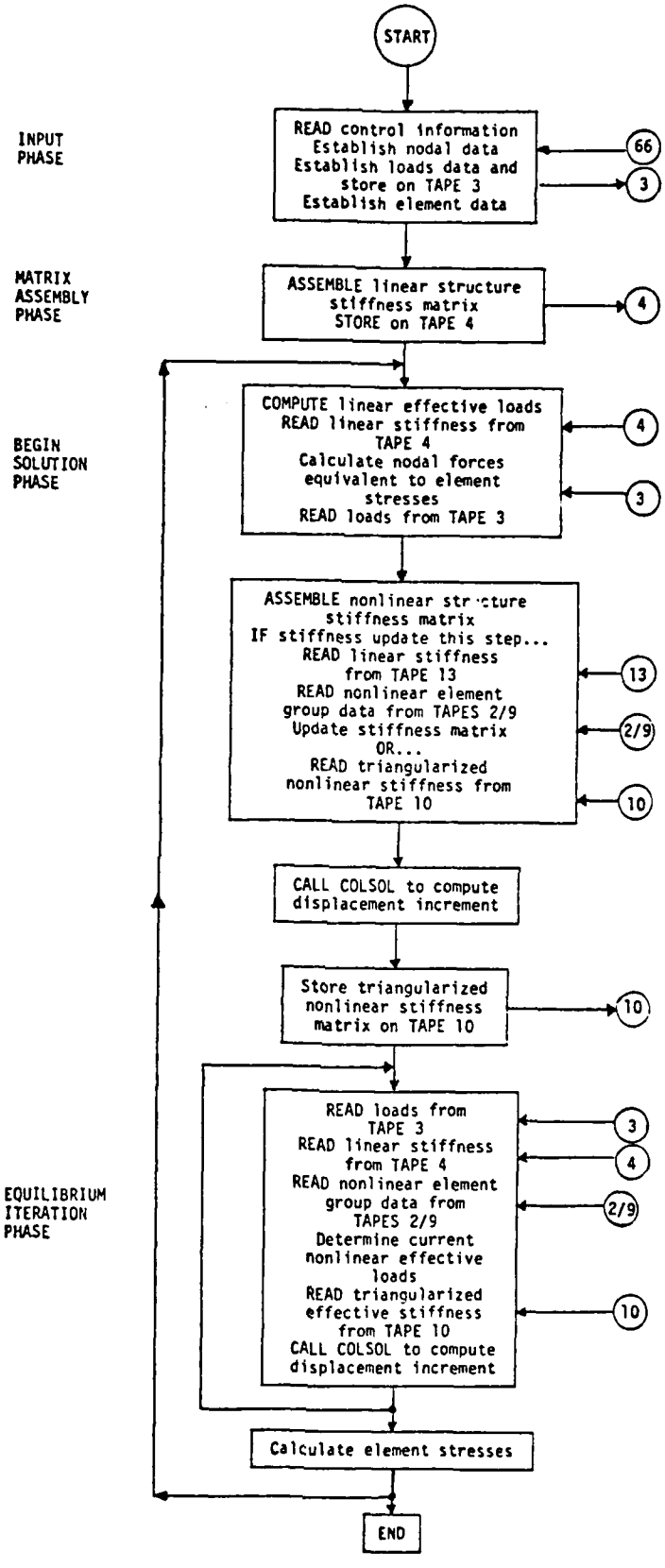

Figure 2.2
NONSAP Flowchart Program Operation
in Nonlinear Static Solution Mode

Moreover, within each load step, solution accuracy may be improved by equilibrium iterations. The interval of load steps at which an equilibrium iteration is to be allowed is also a NONSAP control input.

A solution to the incremental linear equations at each load step is performed by the linear equation solver, COLSOL, which performs Gauss eliminations on the positive definite symmetrical system of equations. This algorithm takes advantage of the banded and sparse structure of the stiffness equations by not processing elements outside a matrix skyline, since they remain zero throughout the computation. The algorithm consists of an LDL^t decomposition of the tangent stiffness matrix into lower triangular, L , and diagonal, D , matrices, followed by a reduction and back substitution of the load vector.

2.2.2.4 NONSAP Element Library

In this section we will briefly describe only those NONSAP element types which are used by HYDROSAP.

The One-Dimensional Truss Element

A one-dimensional truss element, which may be located in three-dimensional space, is used in HYDROSAP to model the thin skin which is on the exterior of some cable fairings. This element has two nodes; it is assumed to have a constant cross-sectional area (which corresponds to the skin thickness in the HYDROSAP plane strain analysis) and to undergo small strains and large displacements.

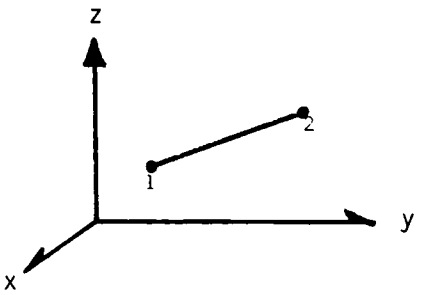

Figure 2.3
A One-Dimensional
Truss Element

The Two-Dimensional Plane Stress/Plane Strain Element

An isoparametric plane strain element, having a variable number of nodes, is used to model the cross-section of the cable fairing. This element may have from three to eight nodes; any of the nodes numbered from five through eight on the sketch may be omitted. A three node element is obtained by setting the coordinates of two nodes for a four node quadrilateral equal to one another. In a plane strain analysis the out-of-plane element thickness is assumed to be unity.

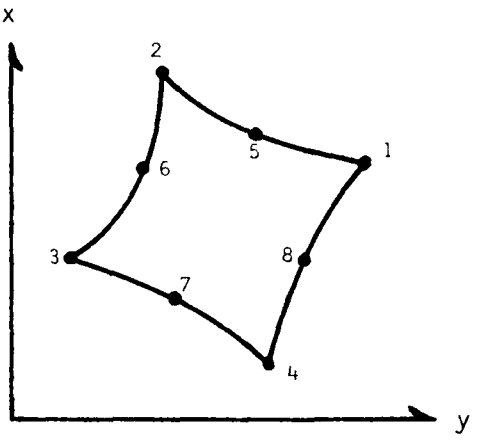

Figure 2.4
A Two-Dimensional Plane Strain Isoparametric Quadrilateral Element

2.3 Sample Computations

In order to illustrate the capabilities of the HYDROSAP software system, in this section we will present the results of some typical computations. In section 2.3.1 will we analyze the behavior of an NACA 0020 section. In section 2.3.2 we will discuss an NACA 65-018 section; and in section 2.3.3 we will explore the sensitivity of the computations to a refinement of the finite element mesh.

2.3.1 The NACA 0020 Profile Section

A hypothetical, three-inch chord faired cable, constructed as an NACA 0020 section, is "towed" through water at 44 fps (34.5 knots). It is assumed to be at an angle of attack of 8°. In the following discussion we designate parameters of the computer model by capitalization. These variables are defined in Appendix A.

Structurally, the towline section is modelled as having a rigid CORE (ECORE = $1x10^6$ psi) extending aft from the leading edge for 3/4" (Y1CORE = 0.0, Y2CORE = 0.75). The afterbody, or TAIL, is assumed to be composed of a relatively flexible rubber-like material (ETAIL = $1x10^4$ psi). The entire fairing section is enclosed by a very flexible skin (ESKIN = $2x10^3$ psi), which is 0.05 inches thick (TSKIN = 0.05). The finite element mesh used to analyze the structural response is generated automatically by the software (MESHC = 11, MESHT = 3). This mesh consists of 48 two-dimensional elements having 57 nodes; the outer SKIN connecting the surface nodes is modelled by 24 one-dimensional elements.

For purposes of the hydrodynamic computations, the fairing's NACA 0020 surface profile is modelled by 35 surface points distributed automatically (HYDROSAP controls: IPANEL = 2, and N = -2 ••• for FOIL03) on the upper and lower fairing surfaces by the software. Viscous effects are included in the computations in each of the HYDROSAP "outer iterations" (ITRSWT = 1).

The effect of the hydrodynamic loading on this flexible symmetric fairing is to induce negative camber. Figure 2.5 summarizes the types of deformations suffered by the fairing cross-section. Evidently the material above the fairing chord is in compression while that below is in tension. The equilibrium trailing edge transverse deflection is approximately 2.3% of the chord.

The negative camber acts to reduce the magnitude of the lift and (nose) moment coefficients significantly. In Figure 2.6 these hydrodynamic coefficients are plotted for each successive pass through the HYDROSAP system. It is evident from the graph that after ten iterations the hydrodynamic loading and structural response are in equilibrium. The fairing's deformation has reduced the lift coefficient by 24%, from C_ℓ = 0.8996 for the undeformed fairing, to C_ℓ = 0.6794 for the deformed fairing. The nose-down moment coefficient, taken about the profile's leading edge, has been reduced by 29%. Figure 2.7 shows the effect that

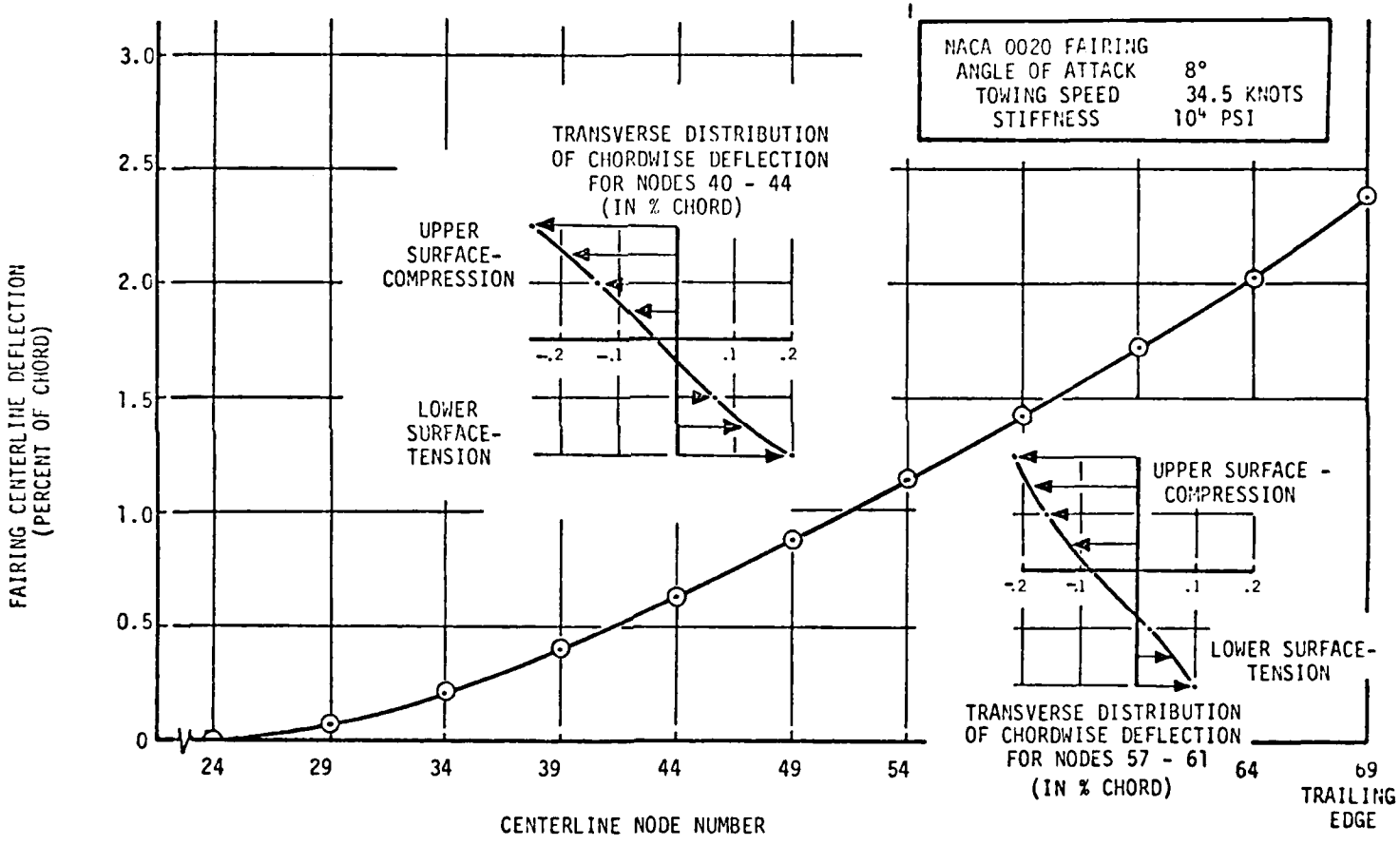

Figure 2.5
Transverse Deflection of Centerline
for a Flexible Cable Fairing

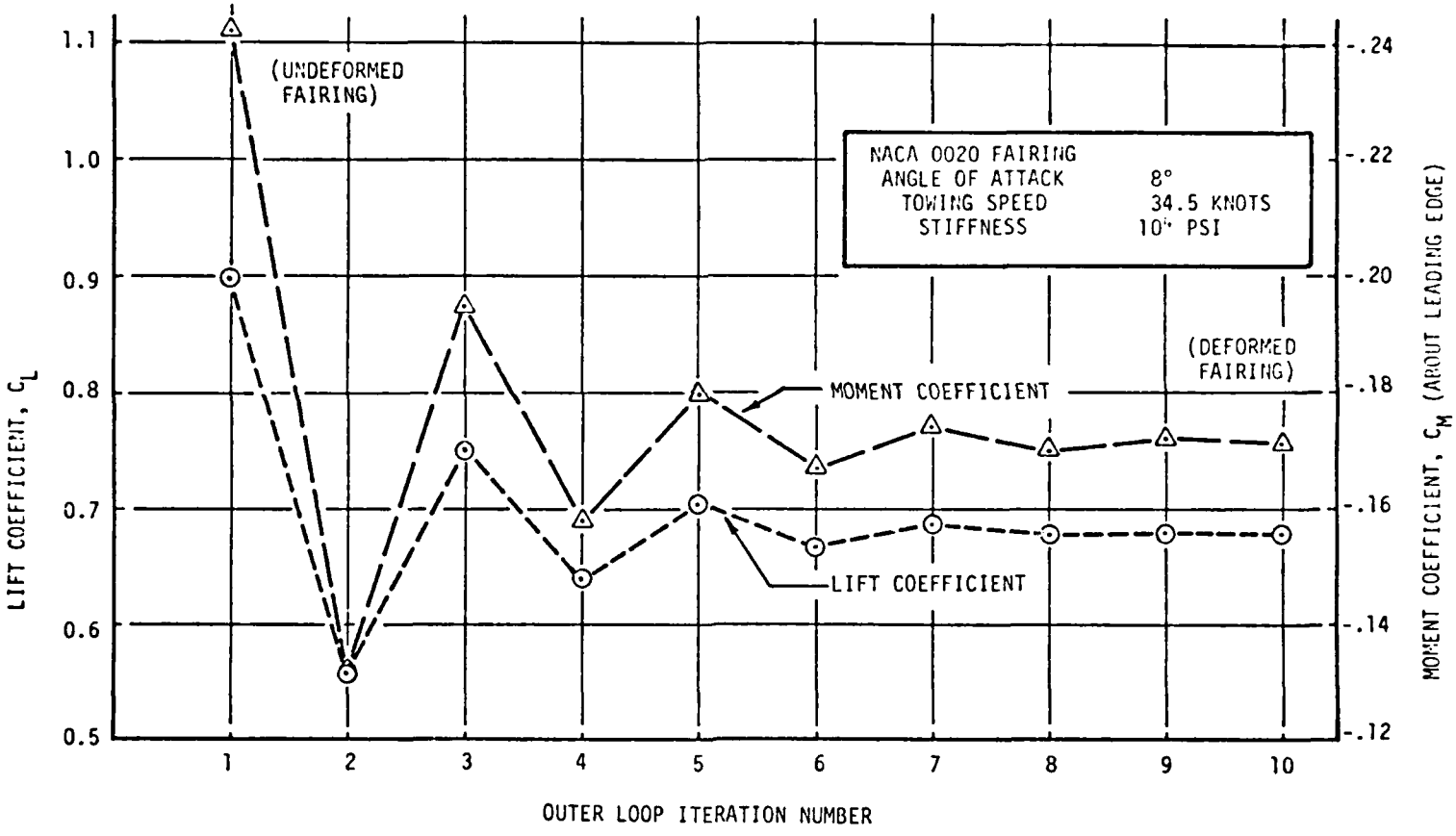

Figure 2.6
Hydrodynamic Coefficients for
a Flexible Cable-Fairing

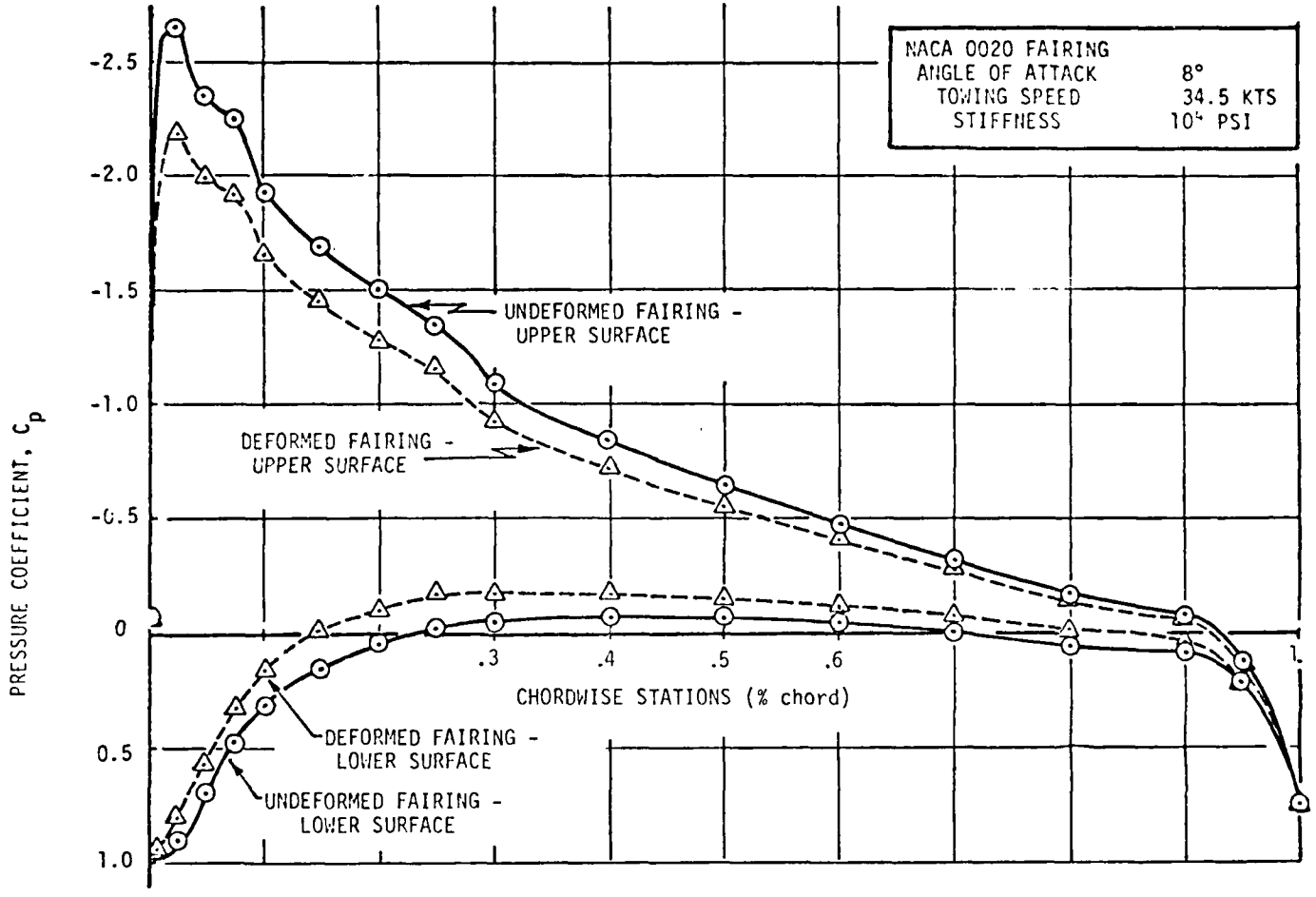

Figure 2.7
Pressure Distributions Over
Undeformed and Deformed Fairings

the modest chordwise deflection of the fairing has on the overall pressure distribution. Pressure coefficients are reduced in magnitude by about 10% to 20% even in the region of the rigid leading edge. The trailing edge deflection evidently makes its presence felt globally over the entire fairing's surface.

2.3.2 The NACA 65-018 Profile Section

We explore the degree of deformation for a flexible NACA 65-018 fairing made entirely of a material with Young's modules (ETAIL) = $1x10^5$ psi. No distinguishable SKIN or CORE are present here. The three-inch section is towed at 44 fps (34.5 kts) through sea-water.

In Figure 2.8 we plot the viscous and potential pressure distributions over the undeformed section at 0° angle of attack. Since the section is symmetric the upper and lower surface pressure distributions are identical, and the profile suffers no deformations. Figures 2.9 and 2.10 show pressure distributions for the deformed and undeformed fairing at 2° and 8° angles of attack, respectively. Figure 2.11 summarizes the angle of attack dependence of the sectional lift, drag, and nose moment coefficients.

Since the NACA 65-018 fairing material is ten times stiffer than that of our NACA 0020 example, the development of negative camber is somewhat less pronounced. Nevertheless, the gradual separation of the deformed and undeformed lift and moment curves in Figure 2.11 underscores the need for careful attention to be given to the local orientation and behavior of the cable sections in a three-dimensional analysis. We note that the drag coefficients are not so sensitive to the pressure induced chordwise deformation of the fairing.

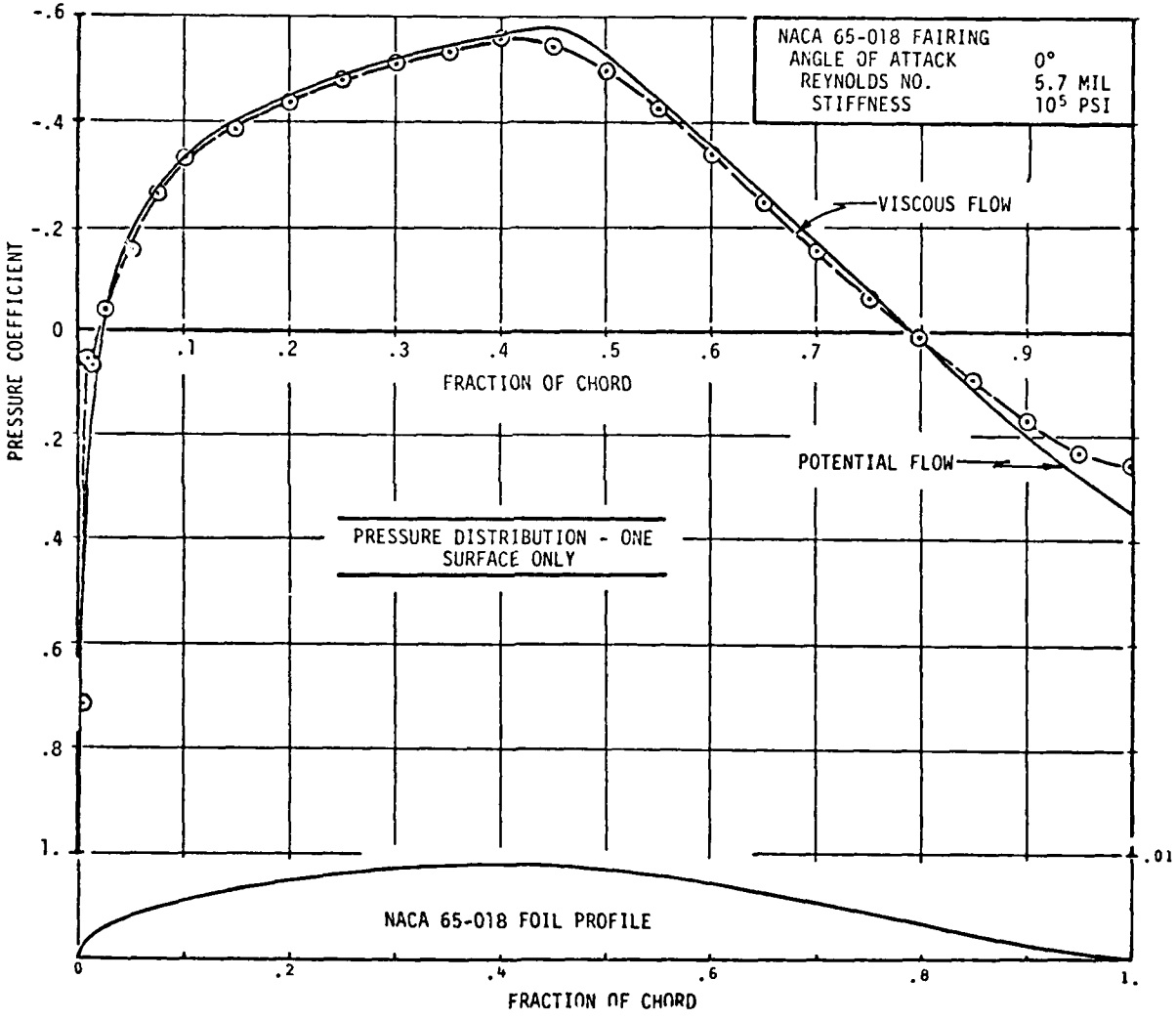

Figure 2.8
Pressure Distribution for Potential and Viscous Fluid Flows
Over a Symmetrical (NACA 65-018) Profile at 0° Angle of Attack

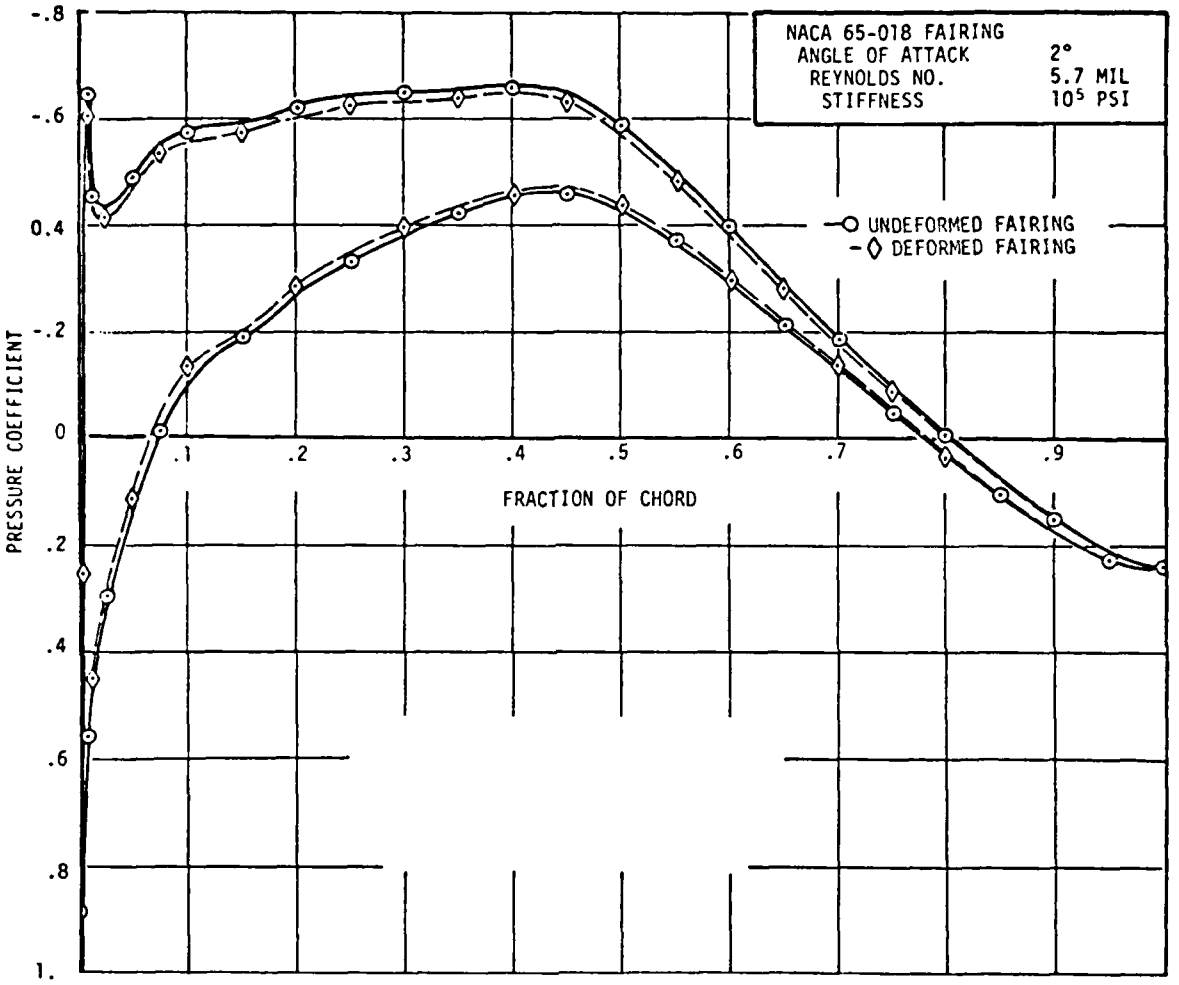

Figure 2.9
Pressure Distribution for the Undeformed
and Deformed Fairing at 2° Angle of Attack

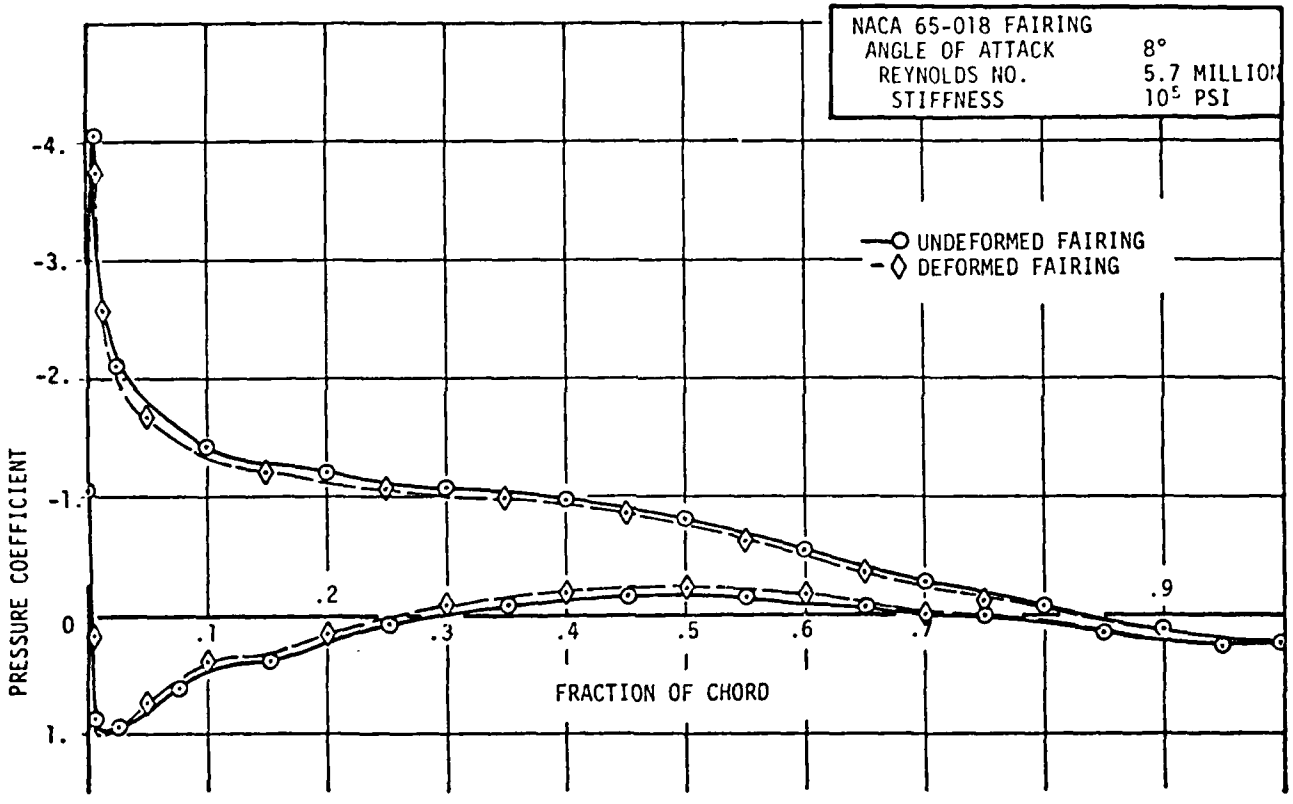

Figure 2.10
Pressure Distribution for the Undeformed and Deformed Fairing at 8° Angle of Attack

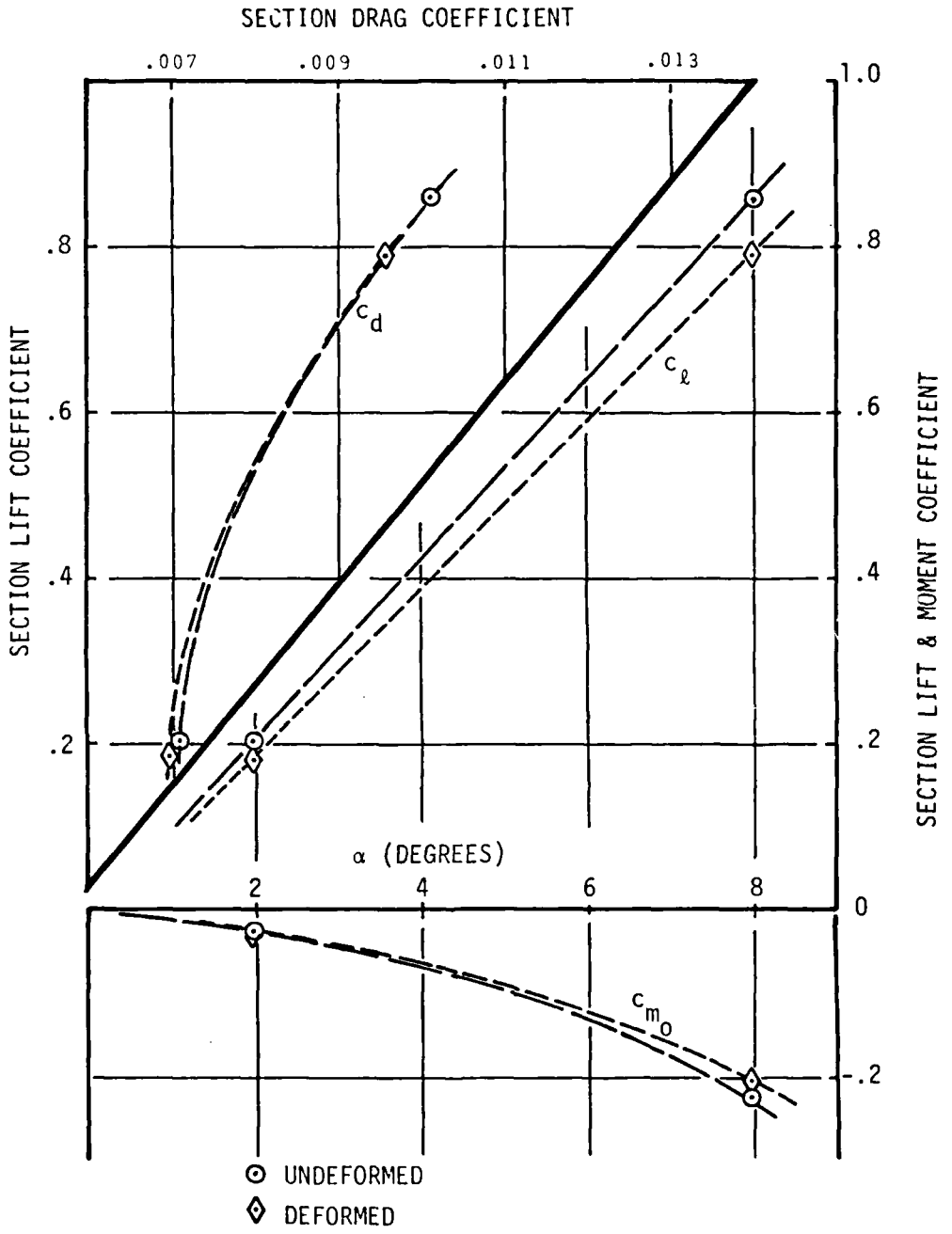

Figure 2.11
Estimated Section Characteristics for the
Deformed and Undeformed NACA 65-018 Profile

2.3.3 An Accuracy Study

Although certain theoretical error estimates are available, to measure the accuracy of a particular finite element solution, in practice it is customary to determine the sensitivity of the numerical solution to the fineness of the finite element mesh by experiment. In this regard we compute the numerical solution for a sequence of finite element meshes; each succeeding mesh being finer than its predecessor.

For this study we use the NACA 0020 fairing of section 2.3.1, but tow it at 4° angle of attack, at 22 fps (13 kts), in seawater. We use the number of nodal points for the mesh as a measure of mesh "fineness". For this analysis the solutions were computed using meshes with 7, 27, 57, 79, and 90 node points. Table 2.1 summarizes the conditions of the tow and the nominal hydrodynamic coefficients for the rigid profile. Table 2.2 gives the variation in trailing edge deflection, the hydrodynamic coefficients, and computer "costs" with the fineness of the mesh. Evidently, increasing the number of nodes from 79 to 90 offers a negligible increase in accuracy. Indeed, even the crudest (and "stiffest") finite element mesh (having only 17 nodes) already accounts for 25% of the reduction in C_ℓ, observed for the deformed fairing modelled with 90 nodes. Obtaining the remaining 15% C_ℓ reduction requires an investment of twice as much computer CPU time.

This completes the brief review of our two-dimensional analysis capabilities. In the next section a description of the three-dimensional analysis development will be presented.

Table 2.1

Nominal Test Values

PROFILE	NACA 0020 section
CHORD (length)	3.0 (in.)
CORE (length)	0.5 (in.)
TAIL MATERIAL MODULUS	10^4 (psi.)
TEST CONDITIONS	
V	22. (fps.)
α	+4. (deg.)
HYDRODYNAMIC COEFFS.	
C_{ℓ}	0.4507
C_{mo}	-0.1223
C_d	0.0086

Table 2.2

Sensitivity Analysis Values

No. of Nodes	Trailing Edge Deflection		Coefficients[1]			No. of Iterations[2]	Run Time[3]	
	Y(in)	Z(in)	C_{ℓ}	C_{mo}	C_d		CPU (mins)	I/O (mins)
17	-0.0016	0.0084	0.4248	-0.1141	0.0085	3	0.50	4.70
27		0.0086	0.4243	-0.1139	0.0085	3	0.68	4.91
57		0.0097	0.4205	-0.1126	0.0084	4	0.90	5.62
79		0.0098	0.4203	-0.1125	0.0084	4	1.07	6.06
90		0.0098	0.4202	-0.1125	0.0084	4	1.15	6.09

NOTES: [1]Coefficients determined from Pressure Distributions;
[2]Outer Loop Iterations, to a coverged solution;
[3]Based on an IBM 360/91 system.

3.0 THE THREE-DIMENSIONAL FLOW-STRUCTURE INTERACTION

3.1 Overview of the Three-Dimensional Problem

In contrast to our focus on the local deformations for a typical cable cross-section, in the two-dimensional study, the object of the three-dimensional study is to determine the global shape of a tow cable. In this case the cable is being influenced by forces from the towed body in addition to the hydrodynamic forces developed on its cross-sectional profiles. For this study the solution methodology is based on a large deformation, small strain theory for the deflections of a heterogeneous, isotropic rod. These deflections are modelled in terms of the three-dimensional motion of a reference curve -- the locus of shear centers for the cable's cross-sections. The cross-section's mechanical properties, such as bending stiffnesses, torsional rigidity, modulus weighted centroids, and shear center locations are the subject of a separate analysis; this is detailed in section 3.2.1, below.

Having reduced the motion of the towing cable to that of the locus of shear centers, the dynamic equations for the displacements of the reference curve are discretized using the finite element technique. We discuss this process and its computer implementation in section 3.2.2.

3.2 Solution Algorithms

3.2.1 Mechanical Properties for a Cable Cross-Section

In order to model a towing cable's dynamical behavior, in terms of the motion of its reference axis, it is necessary to compute for a typical cross-section (or cross-sections, in the case of a non-uniform cable) certain of its mechanical properties.

Referring to Figure 3.1, we shall denote a typical cable cross-section by Ω, and its boundary by $\delta\Omega$. Let us denote by E, ν, and G the sections Young's modulus, Poisson's ratio, and shear modulus, respectively. Note that E, ν, and G may be functions of position within Ω. For example, the heterogeneous cross-section shown in Figure 3.1 consists of a rigid strength member, Ω_1, a soft, flexible afterbody, Ω_2, and a thin sheathing, Ω_3.

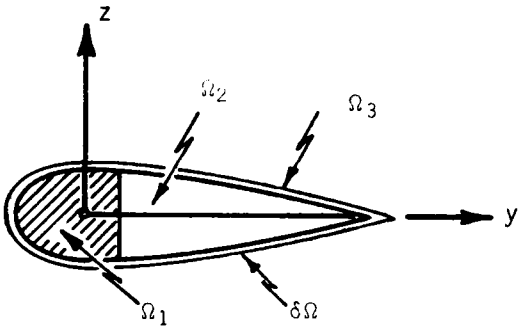

Figure 3.1
A Cable Cross-Section, Ω

We wish to compute the following properties for any representative section:

- modulus weighted area, $\overline{EA} \equiv \int_{\Omega} E \, dy \, dz$
- modulus weighted centroid, $(\bar{y},\bar{z})$ where

$$\bar{y} \equiv \int_{A} Ey \, dy \, dz/\overline{EA}$$

$$\bar{z} \equiv \int_{A} Ez \, dy \, dz/\overline{EA}$$

- bending rigidities,

$$\overline{EI_y} \equiv \int_{\Omega} Ez^2 \, dy \, dz \, ,$$

$$\overline{EI_z} \equiv \int_{\Omega} Ey^2 \, dy \, dz \, ,$$

$$\overline{EI_{yz}} \equiv \int_{\Omega} Eyz \, dy \, dz \, , \text{ and}$$

- torsional rigidity,

$$\overline{GJ} \equiv \int_{\Omega} G(y^2+z^2+y\Psi_{,z}-z\Psi_{,y})\, dy\, dz \ .$$

Here the function Ψ is the St. Venant warping function for the section. The warping function describes the longitudinal (out of plane) deformation for the cross-secion, considered to be a thin prismatic member subject to pure torsion.

By way of explanation, consider the prismatic member shown in Figure 3.2; let it be subject to a twist per unit length of along the axis of the member. The Θ displacement field, for pure torsion, is described as:

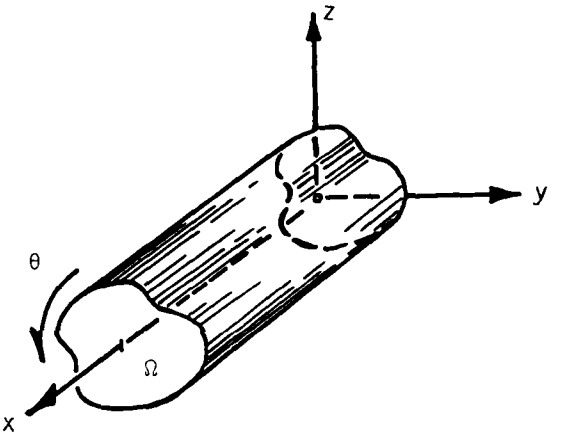

Figure 3.2
A General Prismatic
Member Under Twist, Θ

$$u = \Theta\, \Psi(y,z)$$

$$v = -\Theta \times z \qquad (3.1)$$

$$w = \Theta \times y \ ,$$

where (u,v,w) are displacements, due to Θ, in the (x,y,z) directions. For displacements of the form (3.1), the non-zero strains are:

$$\varepsilon_{yx} = \frac{\partial v}{\partial x} + \frac{\partial u}{\partial y} = \Theta \left(\frac{\partial \Psi}{\partial y} - z\right)$$

and (3.2)

$$\varepsilon_{zx} = \frac{\partial w}{\partial x} + \frac{\partial u}{\partial z} = \Theta \left(\frac{\partial \Psi}{\partial z} + y\right) .$$

The equations of equilibrium, for a heterogeneous, isotropic material, therefore reduce to

$$\frac{\partial}{\partial y}\left[G\left(\frac{\partial \Psi}{\partial y} - z\right)\right] + \frac{\partial}{\partial z}\left[G\left(\frac{\partial \Psi}{\partial z} + y\right)\right] = 0 , \tag{3.3a}$$

in Ω , subject to the boundary condition

$$(\nabla \Psi)\cdot n = z n_y - y n_z , \tag{3.3b}$$

on Ω .

In equation (3.3b), $n = (n_y, n_z)$ is the outward normal to $\delta\Omega$. Clearly, (3.2) and (3.3) determine Ψ only up to a constant; thus we will normalize Ψ by requiring that

$$\int_{\Omega} G \Psi \, dy \, dz = 0 . \tag{3.4}$$

The computer program SHCENT (SHear CENTer) is used to compute the warping function (Ψ) for the airfoil-type cross-sections used for faired towlines whose towing characteristics are to be studied.[2]

---

[2]SHCENT is an adaptation of a code developed by E. M. E. Baumgartner [15].

The finite element method is used to solve equations (3.3). For this, the cable's cross-section is triangulated; Ψ is assumed to be linear on each element of the triangulation; the shear modulus, G, is assumed constant over each element of the triangulation; and a linear equation for the nodal values of Ψ is obtained from the variational form of equations (3.3). We outline this procedure below.

Let ϕ be any function, defined on the cross-section Ω, which together with its gradient is square integrable over Ω. Then the weak (or variational) form of equations (3.3) is

$$\int_{\Omega} \left[G\left(\frac{\partial \Psi}{\partial y} - z\right) \frac{\partial \phi}{\partial y} + G \left(\frac{\partial \Psi}{\partial z} + y\right) \frac{\partial \phi}{\partial z}\right] dy\, dz = 0 . \qquad (3.5)$$

To obtain equation (3.5) we have multiplied (3.3a) by ϕ, integrated over Ω, applied Green's Theorum, and finally taken advantage of (3.3b).

Suppose, for the moment, that Ω is the triangle, T, as in Figure 3.3, and that we consider Ψ to be of the form

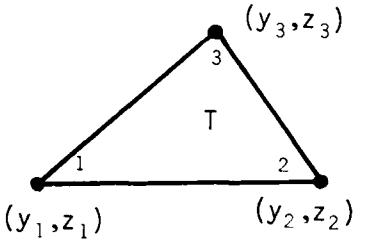

Figure 3.3
Sketch of a Triangular Element with Coordinates (y,z).

$$\Psi(y,z) = \frac{1}{2A} \left(\Psi_1 f_1(y,z) + \Psi_2 f_2(y,z) + \Psi_3 f_3(y,z)\right) \qquad (3.6)$$

where

$$f_i(y,z) \equiv (y-y_j)(z_j-z_k) - (z-z_j)(y_j-y_k) , \qquad (3.7)$$

for, respectively,

$$i=1,2,3$$

$$j=2,3,1$$

$$k=3,1,2$$

and where A is the area of T. We take ϕ in analogous form. Then clearly $\Psi(y_i,z_i) = \Psi_i$, $i=1,2,3$, and Ψ is linear on T.

Next let us observe that

$$\frac{\partial f_i}{\partial y} = z_j - z_k \equiv z_{jk} , \qquad (3.8a)$$

and

$$\frac{\partial f_i}{\partial z} = -(y_j-y_k) \equiv -y_{jk} , \qquad (3.8b)$$

so that

$$\frac{\partial \Psi}{\partial y} = \frac{1}{2A}(\Psi_1 z_{23} + \Psi_2 z_{31} + \Psi_3 z_{12}) , \qquad (3.9a)$$

and

$$\frac{\partial \Psi}{\partial z} = -\frac{1}{2A}(\Psi_1 y_{23} + \Psi_2 y_{31} + \Psi_3 y_{12}) . \qquad (3.9b)$$

Similar equations, of course, hold for ϕ. Thus, equation (3.5) becomes

$$\int_\Omega \frac{G}{2A}\left\{(\Psi_1 z_{23}+\Psi_2 z_{31}+\Psi_3 z_{12})\frac{\partial\phi}{\partial y} -(\Psi_1 y_{23}+\Psi_2 y_{31}+\Psi_3 y_{12})\frac{\partial\phi}{\partial z}\right\}dy$$

$$= \int_\Omega G\left(z\frac{\partial\phi}{\partial y} - y\frac{\partial\phi}{\partial z}\right) dy\, dz\ . \qquad (3.10)$$

Since equation (3.10) must hold for arbitrary ϕ, we select, alternatively, $\phi = f_i$, i=1,2,3. Thus, we have from equation (3.10) three equations for the three unknowns, Ψ_1,Ψ_2,Ψ_3. In matrix form those three equations are

$$K\,\hat{\Psi} = \hat{F} \qquad (3.11)$$

where: $\hat{\Psi}\equiv(\Psi_1,\Psi_2,\Psi_3)^T$, $\hat{F}\equiv(F_1,F_2,F_2)^T$, and $K = (k_{ij})$ for i,j=1,2,3. The matrix K is called the "local stiffness matrix"; its elements are given by

$$k_{11} = G(y_{23}^2+z_{23}^2)/2A\ ,$$

$$k_{12} = k_{21} = G(y_{23}y_{31}+z_{23}z_{31})/2A\ ,$$

$$k_{13} = k_{31} = G\,(y_{23}y_{12}+z_{23}z_{12})/2A\ , \qquad (3.12)$$

$$k_{22} = G(y_{31}^2+z_{31}^2)/2A\ ,$$

$$k_{23} = k_{32} = G(y_{31}y_{12}+z_{31}z_{12})/2A\ ,$$

and

$$k_{33} = G(y_{12}^2+z_{12}^2)/2A\ .$$

The vector of "generalized loads" is given by

$$F_1 = ((\bar{y}\ y_{23}+\bar{z}\ z_{23}) ,$$

$$F_2 = G(\bar{y}\ y_{31}+\bar{z}\ z_{31}) , \qquad (3.13)$$

and

$$F_3 = G(\bar{y}\ y_{12}+\bar{z}\ z_{12}) .$$

Here $(\bar{y}\ ,\ \bar{z})$ are the coordinates of the centroid of the element, T. We retain the shear coefficient, G, in both equation (3.12) and equation (3.13) since the global stiffness matrix and global generalized load vector, for the entire domain Ω, must be assembled from the local values for each element. The local values of the shear constant and element area may vary from element to element.

The global analog of equation (3.11); i.e., the fully assembled matrix problem, is a linear equation for the nodal values of the "best" piecewise linear approximation to Ψ for the given triangulation of Ω [12]. The global problem is solved by elimination, taking advantage, however, of the banded, symmetric and sparse structure of the global stiffness matrix.

3.2.1.1 Torsional Rigidity

The torsional rigidity, $\overline{GJ}$, of the cross-section Ω is defined to be the moment necessary to twist a rod (of cross-section Ω) one radian per unit of length. That is, if the twist of the rod is Θ, then the necessary twisting moment, M, is

$$M = \overline{GJ}\ \Theta . \qquad (3.14)$$

Setting $\Theta = 1$, and writing M in terms of the cross-sectional shear stresses, we have

$$\overline{GJ} = \int_{\Omega} \left(-z\sigma_{yx}+y\sigma_{zx}\right) dy\, dz$$

$$= \int_{\Omega} G\, -z\left(\frac{\partial \Psi}{\partial y}-z\right) + y\left(\frac{\partial \Psi}{\partial z}+y\right) dy\, dz$$

$$= \int_{\Omega} G\, \left(y^2+z^2+y\Psi_{,z}-z\Psi_{,y}\right) dy\, dz\ . \qquad (3.15)$$

Several remarks concerning equation (3.15) are in order.

If G is constant over Ω, we see that

$$\overline{GJ} = G\cdot \int_{\Omega} \left(y^2+z^2+y\Psi_{,z}-z\Psi_{,y}\right) dy\, dz\ . \qquad (3.16)$$

The integral on the right hand side of (3.16) depends only on the shape of Ω, and is called the torsion constant -- usually denoted by J -- for the cross-section. When Ω is a circular section, $\Psi \equiv 0$ over Ω; then J reduces to this section's polar moment of inertia.

3.2.1.2 Bending Rigidities

The bending rigidities, $\overline{EI_{yy}}$, $\overline{EI_{zz}}$, and $\overline{EI_{yz}}$ are computed in SHCENT by calculating the bending rigidities for each triangular element, T, about its own centroid. Using the transfer of axes theorem, these element rigidities are referred to the modulus weighted centroid of the section. Bending rigidities with respect to the global origin -- the modulus-weighted centroid -- and with respect to the shear center are among the program's output.

3.2.1.3 Modulus Weighted Area and Centroid

As with the bending rigidities, the modulus weighted area and weighted centroid, for Ω, are (each) computed by summing over all the triangular elements, T, into which Ω is partitioned; thus:

$$\overline{EA} \equiv \sum_T E_T A_T \ ; \tag{3.17}$$

also

$$\bar{y} \equiv \frac{\sum_T \bar{y}_T E_T A_T}{\overline{EA}} \ , \tag{3.18a}$$

and

$$\bar{z} \equiv \frac{\sum_T \bar{z}_T E_T A_T}{\overline{EA}} \ . \tag{3.18b}$$

3.2.1.4 Shear Center

The shear center for Ω is defined to be that point, in the plane of Ω, at which a transverse point load $P = (P_y, P_z)$, on a rod of cross-section Ω, causes no twist about its longitudinal axis. It is well-known [16] that the resulting normal stress, σ_{xx}, at a point (y,z) in a section, at distance L from the loaded section, is

$$\sigma_{xx} = E(y,z)(C_1 y + C_2 z)L \ , \tag{3.19a}$$

where

$$C_1 \equiv \frac{P_y \overline{EI}_{yy} + P_z \overline{EI}_{yz}}{\overline{EI}_{yy} \cdot \overline{EI}_{zz} - (\overline{EI}_{yz})^2} , \tag{3.19b}$$

$$C_2 \equiv - \frac{P_y \overline{EI}_{yz} + P_z \overline{EI}_{zz}}{\overline{EI}_{yy} \cdot \overline{EI}_{zz} - (\overline{EI}_{yz})^2} . \tag{3.19c}$$

Using the technique in reference [17], it is possible to show that the coordinates, (y_s , z_s) of the shear center are:

$$y_s = C_1' \int_\Omega E(y,z)\ y\Psi(y,z)\ dy\ dz$$

$$+ C_2' \int_\Omega E(y,z)\ z\Psi(y,z)\ dy\ dz , \tag{3.20a}$$

and

$$z_s = C_1'' \int_\Omega E(y,z)\ y\Psi(y,z)\ dy\ dz$$

$$+ C_2'' \int_\Omega E(y,z)\ z\Psi(y,z)\ dy\ dz . \tag{3.20b}$$

Here the constants C_i' are obtained from equations (3.19) when $P_y = 0$, $P_z = 1$; and , C_i'' are the values for $P_y = 1$ and $P_z = 0$. In the SHCENT computer program, the integrals in equations (3.20) are carried out piecewise over Ω , making use of the constancy of $E(y,z)$ and the linearity of $\Psi(y,z)$ over each element T in the triangulation of Ω .

A short user's guide for the SHCENT program is included in Appendix B of this report. Included in this user's guide is a description of the ptogram's input deck, external file requirements, and a flow chart.

3.2.2 The Towline Response

We formulate the equations of motion for the discretized towline in terms of the incremental displacements of the structure as it moves from one (quasi) equilibrium configuration to an adjacent deformed configuration. If we denote by $B(t)$ the deformed state of the towline at time t, then we are interested in the incremental deformation "ΔB", of the towline, from state $B(t)$ to state $B(t+\Delta t)$. We compute the displacements which define ΔB with respect to a local connected coordinate system using a linearized theory. These local deformations are then referred to a fixed global coordinate system by means of local transformations which depend on $B(t)$.

Let us drop, for the moment, the dependence on t and focus on the computation of the incremental displacement, ΔB.

As shown in Figure 3.4, the local incremented displacement field for a prismatic member, B, with cross-section $\Omega(x)$, may be written in terms of the incremental displacements of a reference axis. That is, the displacements of material points in body B can be approximated, over the cross-section, by

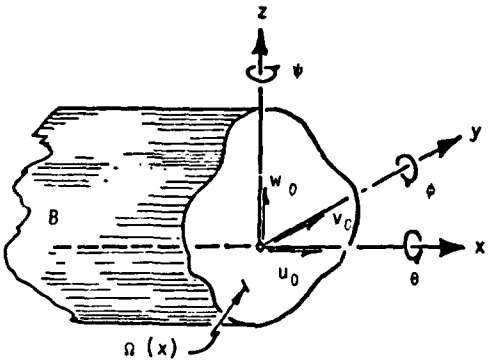

Figure 3.4
A General Prismatic Member

$$u(x,y,z) \equiv u_o(x) - \phi(x)z - \Psi(x)y + \Theta'(x)\,\Psi(x,y,z) \ , \qquad (3.21a)$$

$$v(x,y,z) \equiv v_o(x) - z\Theta(x) \ , \qquad (3.21b)$$

and

$$w(x,y,z) \equiv w_o(x) + y\Theta(x) \ , \qquad (3.21c)$$

where u_o, v_o, w_o are displacements at the reference axis; Θ is the angle of twist; $\phi = dw_o/dx$, and $\Psi = dv_o/dx$ are the bending about the y and z axes, respectively. Also, here, Ψ is the St. Venant warping function for the cross-section; it is obtained by solving the St. Venant torsion problem for $\Omega(x)$, as discussed in section 3.2.1, above. In the sequel, we assume that Ω does not vary along the length of the member.

The strains corresponding to the displacement field (3.21), and subject to the assumption $\Psi = \Psi(y,z)$, are

$$\varepsilon_{xx} = \frac{\partial u}{\partial x} = u_o' - z\phi' - y\Psi' + \Psi\Theta'' \ , \qquad (3.22a)$$

$$\varepsilon_{yy} = \frac{\partial v}{\partial y} = 0 \ , \qquad (3.22b)$$

$$\varepsilon_{zz} = \frac{\partial w}{\partial z} = 0 \ , \qquad (3.22c)$$

$$\varepsilon_{xy} = \frac{\partial v}{\partial x} + \frac{\partial u}{\partial y} = v_o' - z\Theta' - \Psi + \phi'\Psi_{,y} \ , \qquad (3.22d)$$

$$\varepsilon_{yz} = \frac{\partial w}{\partial y} + \frac{\partial v}{\partial z} = 0 \ , \qquad (3.22e)$$

and

$$\varepsilon_{zx} = \frac{\partial u}{\partial z} + \frac{\partial w}{\partial x} = -\phi + \Theta' \Psi_{,z} + w_o' + y\Theta' \ . \qquad (3.22f)$$

Here the primes signify differentiation with respect to x. We relate the non-zero stresses to the strains through the constitutive relations:

$$\sigma_{xx} = (\lambda+2G)\varepsilon_{xx} \ , \qquad (3.23a)$$

$$\sigma_{xy} = G\ \varepsilon_{xy} \ , \qquad (3.23b)$$

and

$$\sigma_{zx} = G\ \varepsilon_{zx} \ . \qquad (3.23c)$$

Here $\lambda = \nu E/(1+\nu)(1-2\nu)$ is the material's Lame' constant, ν is the Poisson ratio, E is the Young's modulus, and $G = E/2(1+\nu)$ is the shear modulus. We will adopt the notation, $\hat{E} \equiv \lambda + 2G$, henceforth.

The internal strain energy increment, V, of body B, subject to the incremental strain field (3.22), and incremental stress field (3.23), is

$$V = \frac{1}{2} \int_B \left\{ \hat{E}\ \varepsilon_{xx}^2 + G\ \varepsilon_{xy}^2 + G\ \varepsilon_{zx}^2 \right\} dx\ dy\ dz \ . \qquad (3.24)$$

Substituting expressions (3.22) into (3.24), and integrating over the cross-section, gives the strain energy in terms of the six functions $u(x)$, $v(x)$, $w(x)$, $\Theta(x)$, $\phi(x)$, and $\Psi(x)$, and the several mechanical properties of the cable's cross-section:

- *modulus weighted area,* $\overline{\hat{E}A} = \int_\Omega \hat{E}\ dy\ dz$;

- modulus weighted centroid,

$$\bar{y} = \frac{1}{\hat{E}A} \int_{\Omega} y \, \hat{E} \, dy \, dz \ ,$$

and

$$\bar{z} = \frac{1}{\hat{E}A} \, z \int_{\Omega} E \, dy \, dz \ ;$$

- bending stiffnesses,

$$\overline{\hat{E}I}_y = \int_{\Omega} z^2 \, \hat{E} \, dy \, dz \ ,$$

$$\overline{\hat{E}I}_z = \int_{\Omega} y^2 \, \hat{E} \, dy \, dz \ ,$$

and

$$\overline{\hat{E}I}_{yz} = \int_{\Omega} yz \, \hat{E} \, dy \, dz \ ;$$

and,

- torsional rigidity,

$$\overline{GJ} = \int_{\Omega} G\left\{y^2+z^2+y\Psi_{,z}-z\Psi_{,y}\right\} dy \, dz \ .$$

We have discussed the computation of these section properties at length in section 3.2.1. There are several other cross-sectional properties which are of interest; we will denote these, generically, using the notation:

$$I(\alpha) \equiv \int_{\Omega} \alpha(y,z)\, dy\, dz \ . \tag{3.25}$$

Thus, for example, we could write

$$\overline{\hat{E}A} \equiv I(\hat{E}) \ ,$$

or

$$\overline{\hat{E}I}_z \equiv I(\hat{E}y^2) \ .$$

Using this notation, and integrating over Ω in equation (3.24), we obtain:

$$V = \frac{1}{2} \int_L \Big\{ \overline{\hat{E}A}\ ((u_o')^2 - 2\bar{z}u_o'w_o'' - 2\bar{y}u_o'v_o'') + 2I(\hat{E}\Psi)u_o'\Theta_x''$$

$$+ 2\,\overline{\hat{E}I}_{yz}\ u_o''w_o'' - 2I(\hat{E}z\Psi)\ \Theta_x''w_o'' - 2I(\hat{E}y\Psi)\Theta_x''v_o''$$

$$+ \overline{\hat{E}I}_y\ (w_o'')^2 + \overline{\hat{E}I}_z\ (v_o'')^2 + I(\hat{E}\Psi^2)(\Theta_x'')^2$$

$$+ \overline{GJ}\ (\Theta')^2 \Big\}\, dx \ . \tag{3.26}$$

In order to discretize the equations of motion for body B , we shall assume that it has been sub-divided into a finite number of parametric elements (which we will again denote by B). Within each of these elements the incremental displacements (of the reference curve) can be modelled as polynomials in the connected coordinate system. The coefficients of the polynomials will be called the generalized displacements, associated with that element. We will model the transverse displacements, v and w , as third order polynomials in the axial coordinate; but the twist, Θ , and the elongation, u , will be linear. Note that for convenience we have dropped the zero subscripts on u,v,w. Thus, we assume:

$$u(x) = u_1\alpha_1(x) + u_2\alpha_2(x) \tag{3.27a}$$

$$v(x) = v_1\beta_1(x) + v_1'\gamma_1(x) + v_2\beta_2(x) + v_2'\gamma_2(x) , \tag{3.27b}$$

$$w(x) = w_1\beta_1(x) + w_1'\gamma_1(x) + w_2\beta_2(x) + w_2'\gamma_2(x) , \tag{3.27c}$$

and

$$\Theta(x) = \Theta_1\alpha_1(x) + \Theta_2\alpha_2(x) ; \tag{3.27d}$$

where, with L being the length of the element, the basis (or shape) functions are

$$\alpha_1(x) = 1 - \frac{x}{L}, \tag{3.28a}$$

$$\alpha_2(x) = \frac{x}{L} , \tag{3.28b}$$

$$\beta_1(x) = 1-3(\frac{x}{L})^2+ 2(\frac{x}{L})^3 \tag{3.28c}$$

$$\gamma_1(x) = L\left\{\frac{x}{L} - 2\left(\frac{x}{L}\right)^2 + \left(\frac{x}{L}\right)^3\right\}, \tag{3.28d}$$

$$\beta_2(x) = 1-3\left(1-\frac{x}{L}\right)^2 + 2\left(1-\frac{x}{L}\right)^3 , \tag{3.28e}$$

and

$$\gamma_2(x) = -L\left\{\left(1-\frac{x}{L}\right) - 2\left(1-\frac{x}{L}\right)^2 + \left(1-\frac{x}{L}\right)^3\right\}. \tag{3.28f}$$

(Recall that x is the longitudinal coordinate for the element). We note that since $v'(x) = \Psi(x)$ and $w'(x) = \phi(x)$, we may write

$$v_i' = \Psi_i, \quad i=1,2$$

and

$$w_i' = \phi_i, \quad i=1,2 .$$

By virtue of the definitions (3.28) -- for the basic functions -- we see that the generalized displacements $(u_i, v_i, w_i, \Theta_i, \Psi_i$, for $i=1,2)$ are the values of the shape functions (3.27) at the node points (points 1 and 2 in Figure 3.5) which define the location of the ends of the "beam". As a consequence of (3.27) and (3.28) we see that $\Theta''=0$, and so the internal energy becomes, in terms of the generalized displacement,

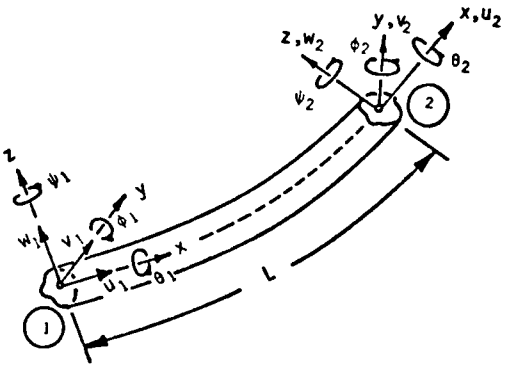

Figure 3.5
A Prismatic Element

$$V = \overline{\hat{E}A}\,\frac{(u_2-u_1)^2}{2L} - \bar{z}\,\overline{\hat{E}A}\left(\frac{u_2-u_1}{L}\right)^2(\phi_2-\phi_1) - \bar{y}\,\overline{\hat{E}A}\left(\frac{u_2-u_1}{L}\right)(\psi_2-\psi_1)$$

$$+ \overline{\hat{E}I}_{yz}\left\{(v_1-v_2)\left[\frac{12}{L^3}(w_1-w_2) + \frac{6}{L^2}(\psi_1+\psi_2)\right]\right.$$

$$\left. + (\phi_1+\phi_2)\left[\frac{6}{L^2}(w_1-w_2) + \frac{2}{L}\left[\psi_2(\phi_1+2\phi_2) + \psi_1(2\phi_1+\phi_2)\right]\right]\right\}$$

$$+ \frac{\overline{\hat{E}I}_y}{2}\left\{\frac{12}{L^3}(w_1-w_2)^2 + \frac{12}{L^2}(w_1-w_2)(\phi_1+\phi_2) + \frac{4}{L}(\phi_1^2+\phi_2^2+\phi_1\phi_2)\right\}$$

$$+ \frac{\overline{\hat{E}I}_z}{2}\left\{\frac{12}{L^3}(v_1-v_2)^2 + \frac{12}{L^2}(v_1-v_2)(\psi_1+\psi_2) + \frac{4}{L}(\psi_1^2+\psi_2^2+\psi_1\psi_2)\right\}$$

$$+ \frac{1}{2}\,\overline{GJ}\,\frac{(\theta_2-\theta_1)^2}{L}\,. \qquad (3.29)$$

Let us denote by $\mu = (u_1, u_2, \theta_1, \theta_2, v_1, \phi_1, v_2, \phi_2, w_1, \psi_1, w_2, \psi_2)^T$ the vector of generalized incremental displacements. We see, then, that the internal energy can be expressed as a quadratic form in the incremental generalized displacements; or,

$$V = \frac{1}{2}\mu^T K \mu\,, \qquad (3.30)$$

where K is the local element stiffness matrix given in Table 3.1.

Table 3.1

A 12 x 12 Beam Stiffness Matrix

	u_1	u_2	θ_1	θ_2	v_1	ϕ_1	v_2	ϕ_2	w_1	ψ_1	w_2	ψ_2
u_1	$\frac{\hat{E}A}{L}$	$-\frac{\hat{E}A}{L}$	0	0	0	$-\frac{\bar{z}\hat{E}A}{L}$	0	$\frac{\bar{z}\hat{E}A}{L}$	0	$-\frac{\bar{y}\hat{E}A}{L}$	0	$\frac{\bar{y}\hat{E}A}{L}$
u_2	$-\frac{\hat{E}A}{L}$	$\frac{\hat{E}A}{L}$	0	0	0	$\frac{\bar{z}\hat{E}A}{L}$	0	$-\frac{\bar{z}\hat{E}A}{L}$	0	$\frac{y\hat{E}A}{L}$	0	$-\frac{\bar{y}\hat{E}A}{L}$
θ_1	0	0	$\frac{GJ}{L}$	$-\frac{GJ}{L}$	0	0	0	0	0	0	0	0
θ_2	0	0	$-\frac{GJ}{L}$	$\frac{GJ}{L}$	0	0	0	0	0	0	0	0
v_1	0	0	0	0	$\frac{12I_z\hat{E}}{L^3}$	$\frac{6I_{yz}\hat{E}}{L^2}$	$-\frac{12I_z\hat{E}}{L^3}$	$\frac{6I_{yz}\hat{E}}{L^2}$	$\frac{12I_{yz}\hat{E}}{L^3}$	$\frac{6I_z\hat{E}}{L^2}$	$-\frac{12I_{yz}\hat{E}}{L^3}$	$\frac{6I_z\hat{E}}{L^2}$
ϕ_1	$-\frac{\bar{z}\hat{E}A}{L}$	$\frac{\bar{z}\hat{E}A}{L}$	0	0	$\frac{6I_{yz}\hat{E}}{L^2}$	$\frac{4I_y\hat{E}}{L}$	$-\frac{6I_{yz}\hat{E}}{L^2}$	$\frac{2I_y\hat{E}}{L}$	$\frac{6I_y\hat{E}}{L^2}$	$\frac{4I_{yz}\hat{E}}{L}$	$-\frac{6I_y\hat{E}}{L^2}$	$\frac{2I_{yz}\hat{E}}{L}$
v_2	0	0	0	0	$-\frac{12I_z\hat{E}}{L^3}$	$-\frac{6I_{yz}\hat{E}}{L^2}$	$\frac{12I_z\hat{E}}{L^3}$	$-\frac{6I_{yz}\hat{E}}{L^2}$	$-\frac{12I_{yz}\hat{E}}{L^3}$	$-\frac{6I_z\hat{E}}{L^2}$	$\frac{12I_{yz}\hat{E}}{L^3}$	$-\frac{6I_z\hat{E}}{L^2}$
ϕ_2	$\frac{\bar{z}\hat{E}A}{L}$	$-\frac{\bar{z}\hat{E}A}{L}$	0	0	$\frac{6I_{yz}\hat{E}}{L^2}$	$\frac{2I_y\hat{E}}{L}$	$-\frac{6I_{yz}\hat{E}}{L^2}$	$\frac{4I_y\hat{E}}{L}$	$\frac{6I_y\hat{E}}{L^2}$	$\frac{2I_{yz}\hat{E}}{L}$	$-\frac{6I_y\hat{E}}{L^2}$	$\frac{4I_{yz}\hat{E}}{L}$
w_1	0	0	0	0	$\frac{12I_{yz}\hat{E}}{L^3}$	$\frac{6I_y\hat{E}}{L^2}$	$-\frac{12I_{yz}\hat{E}}{L^3}$	$\frac{6I_y\hat{E}}{L^2}$	$\frac{12I_y\hat{E}}{L^3}$	$\frac{6I_{yz}\hat{E}}{L^2}$	$-\frac{12I_y\hat{E}}{L^3}$	$\frac{6I_{yz}\hat{E}}{L^2}$
ψ_1	$-\frac{\bar{y}\hat{E}A}{L}$	$\frac{\bar{y}\hat{E}A}{L}$	0	0	$\frac{6I_z\hat{E}}{L^2}$	$\frac{4I_{yz}\hat{E}}{L}$	$-\frac{6I_z\hat{E}}{L^2}$	$\frac{2I_{yz}\hat{E}}{L}$	$\frac{6I_{yz}\hat{E}}{L^2}$	$\frac{4I_z\hat{E}}{L}$	$-\frac{6I_{yz}\hat{E}}{L^2}$	$\frac{2I_z\hat{E}}{L}$
w_2	0	0	0	0	$-\frac{12I_{yz}\hat{E}}{L^3}$	$-\frac{6I_y\hat{E}}{L^2}$	$\frac{12I_{yz}\hat{E}}{L^3}$	$-\frac{6I_y\hat{E}}{L^2}$	$-\frac{12I_y\hat{E}}{L^3}$	$-\frac{6I_{yz}\hat{E}}{L^2}$	$\frac{12I_y\hat{E}}{L^3}$	$-\frac{6I_{yz}\hat{E}}{L^2}$
ψ_2	$\frac{\bar{y}\hat{E}A}{L}$	$-\frac{\bar{y}\hat{E}A}{L}$	0	0	$\frac{6I_z\hat{E}}{L^2}$	$\frac{2I_{yz}\hat{E}}{L}$	$-\frac{6I_z\hat{E}}{L^2}$	$\frac{4I_{yz}\hat{E}}{L}$	$\frac{6I_{yz}\hat{E}}{L^2}$	$\frac{2I_z\hat{E}}{L}$	$-\frac{6I_{yz}\hat{E}}{L^2}$	$\frac{4I_z\hat{E}}{L}$

Corresponding to μ there is a vector, P, which describes the net generalized force increments. Vector P is composed of the net force on body B; i.e., P is determined by the difference between the externally applied loads for the configuration $B+\Delta B$ and the internal resisting loads, corresponding to the deformed configuration B. We model the net forces on B as loads distributed linearly over the length of the element:

$$P_r = P_{r_1}\alpha_1(x) + P_{r_2}\alpha_2(x) \ , \tag{3.31a}$$

and

$$m_r = m_{r_1}\alpha_1(x) + m_{r_2}\alpha_2(x) \ . \tag{3.31b}$$

Here the subscript r represents x, y, or z; and P_r, m_r are the force and moment per unit length acting on B at the reference axis. The work of the external applied loads is given by

$$W = \int_L (p_x u + p_y v + p_z w + m_x \Theta + m_y \phi + m_z \Psi)\, dx \ , \tag{3.32}$$

where u, v, w, Θ, ϕ, and Ψ are given by (3.27). In terms of the components P and μ, W is given by

$$W = \frac{L}{3} p_{x_1} u_1 + \frac{L}{6}(p_{x_1} u_2 + p_{x_2} u_1) + \frac{L}{3} p_{x_2} u_2$$

$$+ \frac{L}{3} m_{x_1} \phi_1 + \frac{L}{6}(m_{x_1} \Theta_2 + m_{x_2} \Theta_1) + \frac{L}{3} m_{x_2} \Theta_2$$

$$+ \frac{17L}{20} p_{y_1} v_1 + \frac{3L}{20} p_{y_1} v_2 - \frac{L^2}{30} p_{y_1} \Psi_2$$

$$+ \frac{3L}{20} p_{y_2} v_1 + \frac{L^2}{30} p_{y_2} \psi_1 + \frac{17L}{20} p_{y_2} v_2$$

$$+ \frac{17L}{20} p_{z_1} w_1 + \frac{3L}{20} p_{z_1} w_2 - \frac{L^2}{30} p_{z_1} \phi_2$$

$$+ \frac{3L}{20} p_{z_2} w_1 + \frac{L^2}{30} p_{z_2} \phi_1 + \frac{17L}{20} p_{z_2} w_2$$

$$+ \frac{(m_{y_1} + m_{y_2})(w_2 - w_1)}{2} + \frac{(m_{y_2} - m_{y_1})(\phi_2 - \phi_1)L}{12}$$

$$+ \frac{(m_{z_1} + m_{z_2})(v_2 - v_1)}{2} + \frac{(m_{z_2} - m_{z_1})(\psi_2 - \psi_1)L}{12} \quad . \qquad (3.33)$$

The external work, W, can therefore be written as the scalar product,

$$W = \mu^T P \quad , \qquad (3.34)$$

between the vector, μ, of generalized displacements, and a vector, P, of generalized loads. Now, for clarity, $P \equiv (P_1, \cdots, P_{12})^T$ is defined by:

$$P_1 = \left(\frac{p_{x_1}}{3} + \frac{p_{x_2}}{6} \right) L \quad ,$$

$$P_2 = \left(\frac{p_{x_1}}{6} + \frac{p_{x_2}}{3} \right) L \quad ,$$

$$P_3 = \left(\frac{m_{x_1}}{3} + \frac{m_{x_2}}{6}\right)L \ ,$$

$$P_4 = \left(\frac{m_{x_1}}{6} + \frac{m_{x_2}}{3}\right)L \ ,$$

$$P_5 = \left(\frac{17P_{y_1}}{20} + \frac{3P_{y_2}}{20}\right)L - \frac{m_{z_1}+m_{z_2}}{2} \ ,$$

$$P_6 = \left(\frac{3P_{y_1}}{20} + \frac{17P_{y_2}}{20}\right)L + \frac{m_{z_1} + m_{z_2}}{2} \ ,$$

$$P_7 = \frac{P_{z_2}L^2}{30} - \frac{\left(m_{y_2}-m_{y_1}\right)L}{12} \ ,$$

$$P_8 = \frac{-P_{z_1}L^2}{30} + \frac{\left(m_{y_2}-m_{y_1}\right)L}{12} \ ,$$

$$P_9 = \left(\frac{17P_{z_1}}{20} + \frac{3P_{z_2}}{20}\right)L - \frac{m_{y_1}+m_{y_2}}{2} \ ,$$

$$P_{10} = \left(\frac{3P_{z_1}}{20} + \frac{17P_{z_2}}{20}\right)L + \frac{m_{y_1}+m_{y_2}}{2} \ ,$$

$$P_{11} = \frac{P_{y_2}L^2}{30} - \frac{\left(m_{y_2}-m_{y_1}\right)L}{12} \ ,$$

and

$$P_{12} = \frac{-P_{y_1} L^2}{30} + \frac{\left(m_{y_2} - m_{y_1}\right) L}{12} \quad . \tag{3.35}$$

It remains to compute the "kinetic energy", T, of the displacement increment from state B to state $B+\Delta B$; i.e.,

$$T = \frac{1}{2} \int_B \rho(x,y,z) \left\{ (\dot{u})^2 + (\dot{v})^2 + (\dot{w})^2 \right\} dx\, dy\, dz \quad . \tag{3.36}$$[3]

The substitution of equations (3.26) into (3.33), with the application of(3.27) and (3.28), results in an equation of the form:

$$T = \frac{1}{2} \dot{\mu}^T M_c \dot{\mu} \tag{3.37}$$

where the consistent mass matrix, M_c, is a result of the integration of the material density, ρ, against the various products of shape functions arising as a consequence of (3.36). We note that M_c is a "full" matrix. In computer implementations of the method it is customary to replace M_c by a diagonal lumped mass matrix, M, in the interests of speeding the numerical integration of the equations of motion. The diagonal elements of this matrix, M, are given by:

$$M_{1,1} = \frac{\rho A L}{2} \quad ,$$

$$M_{2,2} = \frac{\rho A L}{2} \quad ,$$

$$M_{3,3} = \frac{\rho L I_x}{2} \quad ,$$

---

[3]The superscript dot denotes a time derivative; $(\dot{*}) \equiv \frac{d}{dt}(*)$.

$$M_{4,4} = \frac{\rho L I_x}{2} ,$$

$$M_{5,5} = \frac{\rho A L}{2} ,$$

$$M_{6,6} = \frac{\rho A L^3}{24} + \frac{\rho L I_z}{2} ,$$

$$M_{7,7} = \frac{\rho A L}{2} ,$$

$$M_{8,8} = \frac{\rho A L^3}{24} + \frac{\rho L I_z}{2} ,$$

$$M_{9,9} = \frac{\rho A L}{2} ,$$

and

$$M_{10,10} = \frac{\rho A L^3}{24} + \frac{\rho L I_z}{2} . \qquad (3.38)$$

The kinetic energy, T, potential energy, V, and external work, W, for the entire structure, are assembled from the local values by means of the local to global element transformation matrices, E_B. Using the subscript B for elemental quantities, and the subscript G for global quantities, we may write, formally:

$$T = \sum_B \frac{1}{2} \dot{\mu}_B^T E_B^T M_B E_B \mu_B \equiv \frac{1}{2} \dot{\mu}_G^T M_G \mu_G ,$$

$$V = \sum_B \frac{1}{2} \mu_B^T E_B^T K_B E_B \mu_B \equiv \frac{1}{2} \mu_G^T K_G \mu_G ,$$

and

$$W = \sum_B \mu_B^T E_B^T E_R^T P_B \equiv \mu_G^T P \quad . \tag{3.39}$$

In the sequel we suppress the subscript G ; thus, all generalized vectors and matrices will be global quantities unless otherwise noted.

Let us define the Lagrangian, L , for this deformation increment to be

$$L = T-V+W \quad . \tag{3.40}$$

Applying Hamilton's Principle, we require that

$$J(\mu) \equiv \int_t^{t+\Delta t} (T-V+W)\, ds \tag{3.41}$$

be extremized by the solution vector, μ . Setting $\partial J/\partial \mu = 0$ gives Langrange's equations:

$$\frac{d}{dt}\frac{\partial L}{\partial \dot{\mu}} - \frac{\partial L}{\partial \mu} = 0 \ . \tag{3.42}$$

However, since we know that

$$\frac{\partial L}{\partial \mu} = - k\mu + P \ ,$$

$$\frac{\partial L}{\partial \dot{\mu}} = M\dot{\mu} \ ,$$

and

$$\frac{d}{dt}\frac{\partial L}{\partial \dot{\mu}} = M\ddot{\mu} \ ,$$

then equation (3.42) implies that

$$M\ddot{\mu} + k\mu = P \ . \tag{3.43}$$

We integrate equation (3.42) using the implicit Newmark beta method [11] as follows: Introducing the notation,

$$\mu(t) = \mu_0 \ , \ (\equiv 0 \ , \text{ from the definition of } \mu \ ) \ ,$$

$$\mu(t+\Delta t) = \mu_1 \ ,$$

$$\dot{\mu}(t) = \dot{\mu}_0 \ ,$$

$$\dot{\mu}(t+\Delta t) = \dot{\mu}_1 \ ,$$

$$\mu(t) = \mu_0 \ ,$$

and

$$\ddot{\mu}(t+\Delta t) = \ddot{\mu}_1 \ ,$$

We express the displacement increment, and velocity, at the end of the time step by

$$\mu_1 = \mu_0 + \dot{\mu}_0 \Delta t + (\tfrac{1}{2} - \beta)\ddot{\mu}_0 \Delta t^2 + \beta \ddot{\mu}_1 \Delta t^2 \ ,$$

and

$$\dot{\mu}_1 = \dot{\mu}_0 + \frac{\ddot{\mu}_0 + \ddot{\mu}_1}{2} \Delta t \ . \tag{3.44}$$

We seek μ_1 , $\dot{\mu}_1$ and $\ddot{\mu}_1$, given $\dot{\mu}_0$, $\ddot{\mu}_0$ and $\mu_0(=0)$. Premultiplying the first of equations (3.44) by M , and solving for $M\ddot{\mu}_1$, we obtain from (3.43)

$$(K + \frac{1}{\beta \Delta t^2} M)\mu_1 = P + \frac{1}{\beta \Delta t} M (\dot{\mu}_0 + \frac{1-2\beta}{2\beta} \ddot{\mu}_0) \ . \tag{3.45}$$

Let us define an effective stiffness matrix, $\hat{K}$, by

$$\hat{K} \equiv K + \frac{1}{\beta \Delta t^2} M \ ,$$

and an effective load vector by

$$\hat{P} = \frac{1}{\beta \Delta t} M(\dot{\mu}_0 + \frac{1-2\beta}{2\beta} \ddot{\mu}_0) \ .$$

Then (3.45) takes on the form

$$\hat{K}\mu_1 = \hat{P} \ . \tag{3.46}$$

After computing μ_1 , using an elimination scheme which takes advantage of the symmetric, banded, and sparse structure of $\hat{K}$, we compute $\ddot{\mu}_1$ and $\dot{\mu}_1$ from (3.44): thus,

$$\mu_1 = \frac{1}{\beta \Delta t^2}\left\{\mu_1 - \dot{\mu}_0 \Delta t - (\frac{1}{2} - \beta)\Delta t^2 \ddot{\mu}_0\right\} \tag{3.47}$$

and

$$\dot{\mu}_1 = \dot{\mu}_0 + \frac{1}{2}\Delta t\left\{\ddot{\mu}_0 + \ddot{\mu}_1\right\}. \tag{3.48}$$

Note that the matrix $\hat{K}$ depends on the current geometry through the local-global element transformation matrices. The displacements, μ_1 are used to update those local transformations, which in turn are used to update $\hat{K}$. Also, the net load vector, P , is updated based on the increment in external loads and the new internal loads at time, $t+\Delta t$, or:

$$P(t+\Delta t) = P_{ext}(t+\Delta t) - P_{int}(t+\Delta t), \qquad (3.49)$$

where the internal resisting load is given by

$$P_{int}(t+\Delta t) = P_{int}(t) + \hat{K}\mu_1 \ . \qquad (3.50)$$

The external loads, $P_{ext}(t+\Delta t)$, are a combination of user-supplied external loads and hydrodynamic loads which are themselves dependent on the current deformed state of the cable.

The hydrodynamic loads are computed in terms of the local components of the velocity of the fluid flowing past each element of the cable. (For the purposes of this discussion we will denote the local coordinates within each element by $(\hat{x},\hat{y},\hat{z})$ as shown in Figure 3.6). The $\hat{x}$ axis of the cable element lies along the locus of shear centers. With respect to this locus the aerodynamic center (A.C.) and the modulus-weighted centroid (c.g.) are described by coordinates (y_{ac},z_{ac}) and (y_{cg},z_{cg}) , respectively. For each cable element there is a transformation matrix, E_B , which transforms the local coordinates to the global system; this is indicated in Figure 3.7.

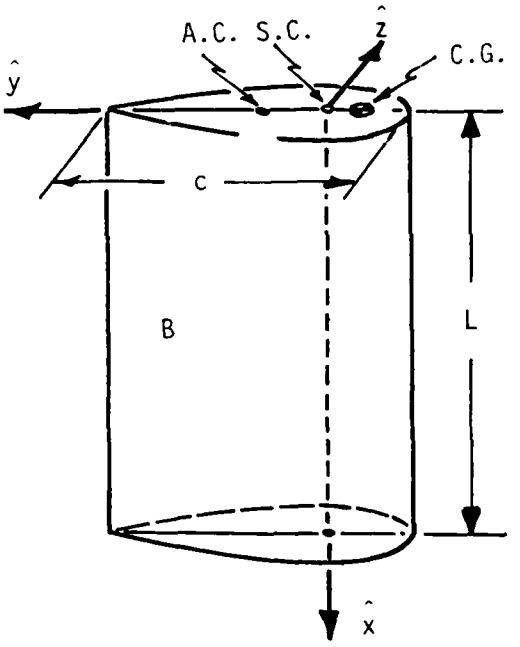

Figure 3.6
Local Coordinate for Element B

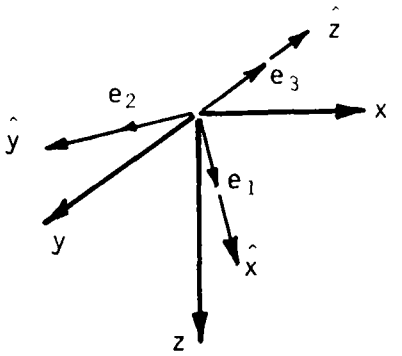

Figure 3.7
Sketch Showing Global/Local Coordinates

If e_1, e_2, e_3 are unit vectors along the local $\hat{x}, \hat{y}, \hat{z}$ axes, then E_B is given by

$$E_B = \begin{bmatrix} e_{11} & e_{12} & e_{13} \\ e_{21} & e_{22} & e_{23} \\ e_{31} & e_{32} & e_{33} \end{bmatrix} \qquad (3.51)$$

where $e_i = (e_{1i}, e_{2i}, e_{3i})^T$ is in global coordinates.

Let V be the velocity vector of the fluid flow relative to the cable. Let the velocity have global coordinates, $V = (V_1, V_2, V_3)^T$, and let the corresponding local coordinates (at element B) be expressed by

$$E_B^T \begin{bmatrix} V_1 \\ V_2 \\ V_3 \end{bmatrix} = \begin{bmatrix} \hat{V}_1 \\ \hat{V}_2 \\ \hat{V}_3 \end{bmatrix} . \qquad (3.52)$$

Clearly, $\hat{V}_1 e_1$ is the local spanwise component of V, the velocity; and

$$U \equiv V - \hat{V}_1 e_1 \qquad (3.53)$$

is the local normal component of V.

The local angle of attack, α, is given by

$$\alpha = \tan^{-1} \left[\frac{\hat{V}_3}{\hat{V}_2} \right] . \qquad (3.54)$$

The local values of hydrodynamic lift (per unit length), normal drag (per unit length), tangential drag (per unit length), and twisting moment (per unit length) about the hydrodynamic center are given, respectively, by

$$L = (C_{L_\alpha} \cdot \alpha) Q \cdot C$$

$$D_N = C_{D_N} \cdot Q \cdot C \ ,$$

$$D_T = C_{D_T} \cdot Q^* \cdot C \ ,$$

and

$$M_{HC} = C_{M_{HC}} \cdot Q \cdot C^2 \ , \qquad (3.55)$$

where

$C \equiv$ section chord length,

$$Q = \frac{1}{2}\rho |U|^2 \ ,$$

$$Q^* = \frac{1}{2}\rho |V_1|^2 \ ,$$

C_{L_α} = section lift-curve slope,

C_{D_N} = normal drag coefficient,

C_{D_T} = tangential drag coefficient,

and

$C_{M_{HC}}$ = moment coefficient about the hydrodynamic center.

The local components $(\hat{F}_1,\hat{F}_2,\hat{F}_3)$ of these hydrodynamic forces are

$$\hat{F}_1 = \sin(\hat{V}_1)D_T ,$$

$$\hat{F}_2 = D_N \cos\alpha - L \sin\alpha ,$$

and

$$\hat{F}_3 = D_N \sin\alpha + L \cos\alpha . \tag{3.56}$$

Consequently the global components (F_1,F_2,F_3) are given by

$$\begin{bmatrix} F_1 \\ F_2 \\ F_3 \end{bmatrix} = E_B \begin{bmatrix} \hat{F}_1 \\ \hat{F}_2 \\ \hat{F}_3 \end{bmatrix}. \tag{3.57}$$

Since the hydrodynamic loads act at the hydrodynamic center of the section, they contribute to the moment about the $\hat{x}$ axis; consequently,

$$\hat{M}_{\hat{x}} = (y_{HC}\hat{F}_3 - z_{HC}\hat{F}_2) + M_{HC} . \tag{3.58}$$

The global components (M_x, M_y, M_z) of this moment are given by

$$\begin{bmatrix} M_x \\ M_y \\ M_z \end{bmatrix} = E_B \begin{bmatrix} \hat{M}_{\hat{x}} \\ 0 \\ 0 \end{bmatrix} . \qquad (3.59)$$

Of considerable interest, for an interpretation of the cable's behavior, are the trail angle, ϕ , and kite angle, θ . If we regard the global x-z plane as the plane of the tow, then we define ϕ and θ from

$$\cos \phi = e_{11} ,$$

$$\sin \phi \sin \theta = e_{21} ,$$

and

$$\sin \phi \cos \theta = e_{31} . \qquad (3.60)$$

We note that for $e_{21}^2 + e_{31}^2 = 0$ the kite angle is not defined, $|\cos\alpha| = 1$, thus the cable is horizontal.

We remark that with this formulation we can easily take into account the pressure distribution-induced distortions of those cable element cross-sections which experience a local flow at a non-zero angle of attack. That is, using the results of the two-dimensional analysis (c.f. section 2 above) we let the hydrodynamic coefficients depend on the local flow velocity and the instantaneous angle of attack. Thus, e.g.,

$$C_{D_N} \equiv C_{D_N}(\alpha, V) ; \qquad (3.61)$$

such a function could be given in tabular form or introduced through the use of interpolating polynomials. This feature is not incorporated into the present version of the three-dimensional program, TOWLINE, due to constraints on the computer budget for the present study. An extensive series of two-dimensional HYDROSAP analyses would be required in order to construct the tables for each individual cable cross-section, under investigation.

Notwithstanding, some samples of the TOWLINE computations are discussed in section 3.3.2 below.

3.3 Sample Computations

3.3.1 Cross-Section Mechanical Properties

We will seek, for this example, the cross-sectional mechanical properties of an NACA 0020 cable section, having a three-inch chord. The section has a glass fibre strength member (core) in the nose, and a flexible afterbody made of rubber (tail), as shown in Figure 3.8. Let us suppose, in addition, that the core extends aft of the section's nose to the 20% chord station. The core material is isotropic, with a Young's modulus of $E=9.4\times10^{6}$ psi; also, suppose it has a shear modulus $G=3.615\times10^{5}$ psi. The material constants for the tail are assumed to be $E=3\times10^{3}$ psi, and $3G=1.154\times10^{3}$ psi.

We triangulate the cross-section as shown in Figure 3.8. Fifty-eight triangular elements, defined by 46 node points, make up the finite element mesh. We expect, due to the large ratios of the material properties (for the nose compared to those of the tail) that the mechanical properties of the section will essentially be those of the nose. Our expectations are confirmed by the results shown in Table 3.2, where we list the mechanical properties of the heterogeneous section, the core alone, and for a homogeneous section having the material properties of the core throughout the entire section. Clearly, the concentration of

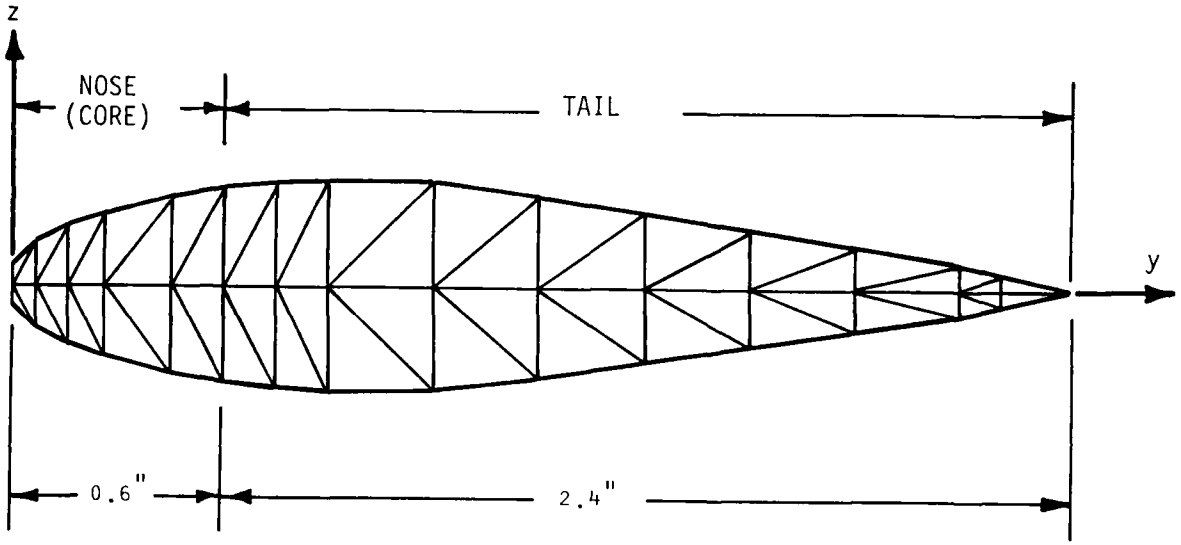

Material Properties

$E = 9.4 \times 10^6$ psi
$G = 3.6 \times 10^5$ psi

$E = 3 \times 10^3$ psi
$G = 1.15 \times 10^3$ psi

Figure 3.8
Details of the Triangulation Used to Determine the Shear Center and Torsional Rigidity of an NACA 0020 Fairing

Table 3.2

Cross-sectional Properties of the NACA 0020

Cable Fairing

MECHANICAL PARAMETER	THE HETEROGENEOUS SECTION	CORE ALONE	THE HOMOGENEOUS SECTION
Modulus-weighted Centroid (in).			
$\bar{y}$	0.35136	0.34996	1.2623
$\bar{z}$	0.	0.	0.
Shear Center (in.)			
y_s	0.36018	0.35898	1.1129
z_s	0.	0.	0.
Modulus-weighted Bending Stiffness (in^4)			
$\overline{EI}_{yz}/E^*$ ([1])	4.745×10^{-3}	4.738×10^{-3}	2.521×10^{-2}
$\overline{EI}_{zz}/E^*$	6.925×10^{-3}	6.409×10^{-3}	6.044×10^{-1}
Modulus-weighted Torsional Rigidity (in^4)			
$\overline{GJ}/_{G^*}$ ([2])	8.978×10^{-3}	8.938×10^{-3}	1.085×10^{-1}
Modulus-weighted Area (in^2)			
$\overline{EA}/E^*$	0.25504	0.25470	1.2252

([1]) $E^* = 9.4\times10^6$ psi ([2]) $G^* = 3.62\times10^6$ psi

Young's modulus and shear modulus in the core material enables one to essentially ignore the contributions to stiffness, etc., due to the tail material.

3.3.2 The Towline's Response

The TOWLINE computer program is designed to determine the (static) equilibrium position of an integrated (faired) towline under steady towing conditions. This is to be accomplished by simulating the dynamic response of the tow cable to the hydrodynamic forces induced by the towing platform and the cable's three-dimensional dynamic response. The TOWLINE code is an adaptation of a program written by IITRI [18] to study the large displacements and deformations incurred in vehicle collisions.

In this section we present the results of computations on a model cable problem which was used for program development. In order to remain within the constraints on computer resources, the model problem has only nine elements and has a higher stiffness-to-length ratio than would be found in an operational towline. The results are intended only to demonstrate the qualitative behavior of faired tow cables; and, to demonstrate the capabilities of the TOWLINE program.

Suppose that a 108-inch faired cable is suspended, vertically, in a 264 in/sec steady fluid flow, and that the cable is subject to a 2.64 in/sec cross-current. By these conditions, the cable's cross-sections have an initial angle of attack of 0.575° with respect to the remote resultant flow. The cable's upper end (point) is "fixed" in space, but free to swivel. No depressor is fixed to the cable's lower endpoint, which is completely unconstrained in space. The initial global configuration of the cable is shown in Figure 3.9. Although the cable is of a composite construction, we assume that effective homogeneous mechanical properties have been determined (using program SHCENT as discussed in section 3.1, above). These mechanical properties of the cable are summarized as follows:

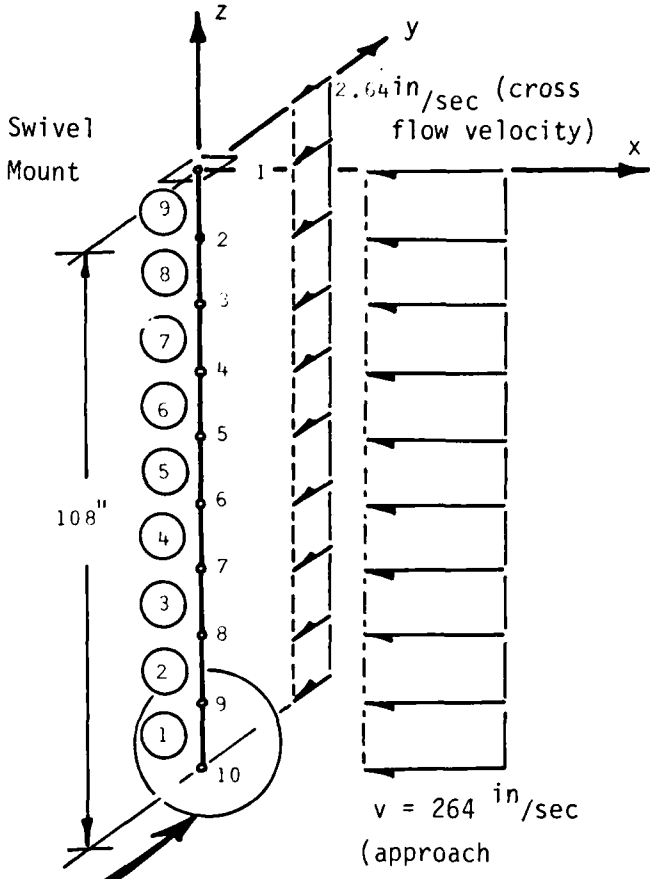

Figure 3.9A
The Global Coordinate System

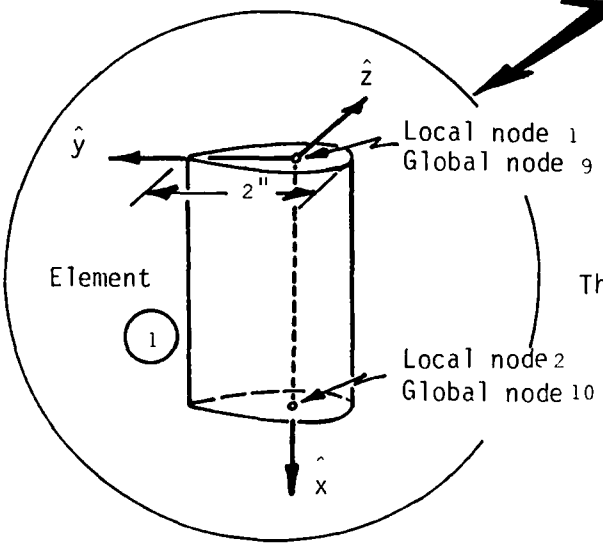

Figure 3.9B
The Local Coordinate System

- cable density; 3.7×10^{-4} lbf-sec^2/in^4
- weight in water; 8.46×10^{-2} lbf/in
- modulus weighted area; $\overline{EA} = 8 \times 10^5$ lbf
- position of modulus weighted centroid; 0.5 in. aft of leading edge
- modulus weighted moments of inertia:

$$\overline{EI}_{yy} = 1 \times 10^4 \text{ lbf-in}^2 ,$$

$$\overline{EI}_{zz} = 4.67 \times 10^5 \text{ lbf-in}^2 ,$$

$$\overline{EI}_{yz} = 0 \text{ (a symmetric section)}$$

and

- torsional rigidity;

$$\overline{GJ} = 1.64 \times 10^4 \text{ lbf-in}^2 .$$

We assume that (with negligible error) that the shear center and modulus-weighted centroid coincide. The hydrodynamic properties of the cable are parameterized by:

- Chord length of the cross-section; c=2 in.

- Lift curve slope; $C_{L_\alpha} \cong 2\pi/\text{rad}$
- Normal drag coefficient; $C_{D_N} \cong 0.01$
- Tangential drag coefficient; $C_{D_T} \cong 0.01$
- Moment coefficient about the aerodynamic center; $C_{M_{AC}} = 0$
- *Position of the aerodynamic center (A.C.); 0.10 in. aft of the modulus weighted centroid.*

We model the cable using nine beam elements, each of which is 12 inches long. A time step of $\Delta t = .01$ sec. has been used for the integration procedure. In Figures 3.10A and 3.10B we show the successive states of deformation, for the cable, during the first ten integration steps. We remark that the "equilibrium" position of the cable has (of course) not been attained in only ten time steps.

Referring to Figure 3.10A, we note that under the influence of the 264 in/sec. tow velocity, the cable begins to move aft; and, the largest trail angles are near the tow point, as expected. We see, however, that between the eighth and tenth integration steps a wave-like motion has developed.[4] While the free end of the cable continues moving aft, cable elements 9, 8, 7, (and possibly 6) (nodes 1, 2, 3, 4, 5)) are moving forward. Superimposed on this swinging motion, aft, is a higher frequency vibratory motion in the vertical direction. This is typified by the x-z position of node 10.

From Figure 3.10B we see that the cable, under influence of the -2.64 in/sec transverse current, is "fluttering" about the x-z plane of the tow. In integration steps 1 through 4 the cable moves -- nearly as a rigid body -- with the cross-current. Inertia and angle of attack

---

[4] This "whipping" effect was even more pronounced in longer cables; in many instances dominating the responses and sending the program to (numerical) divergence.

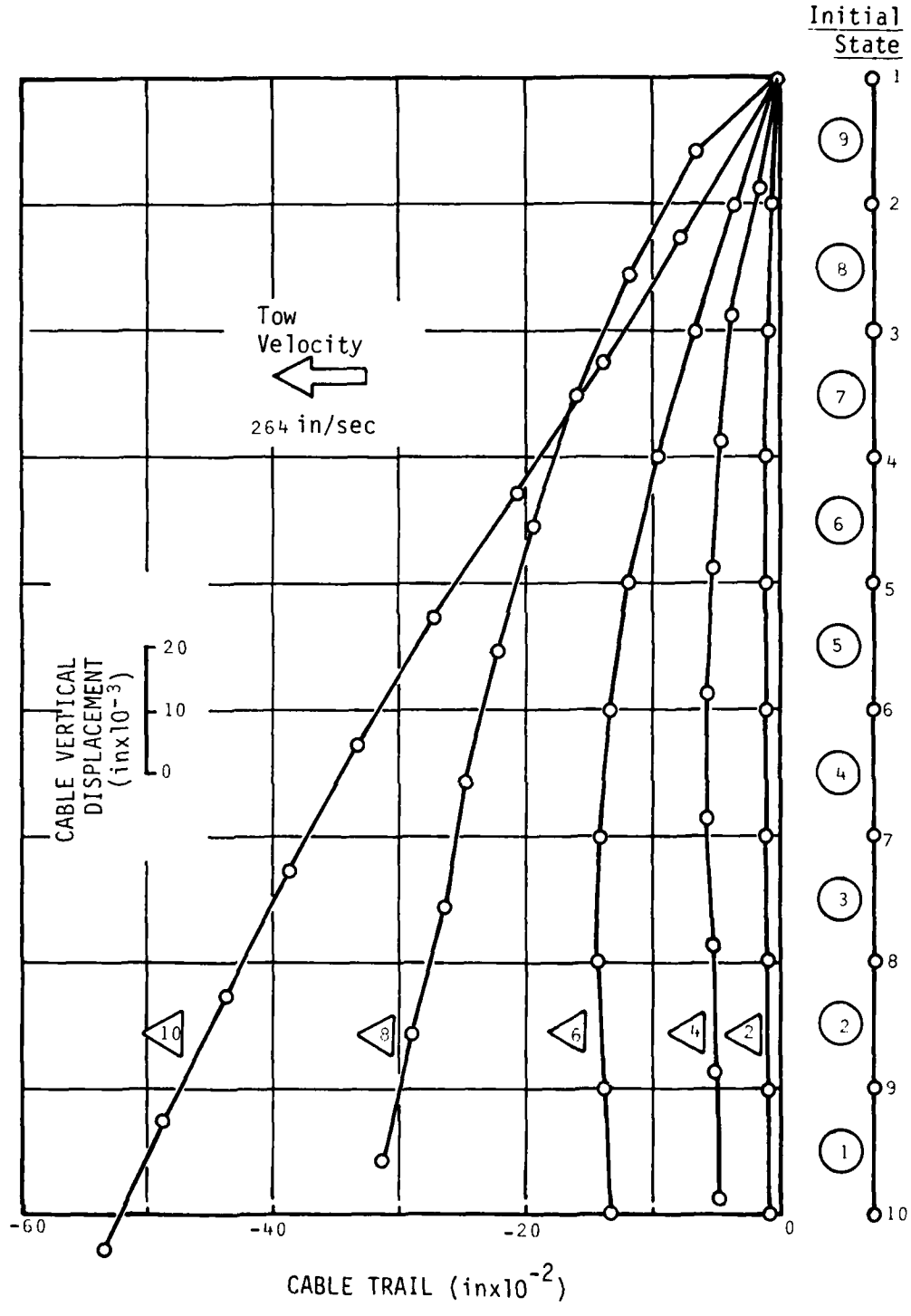

Figure 3.10A
Cable Nodal Relative Positions, in the Plane of the Tow (the x, z Plane)

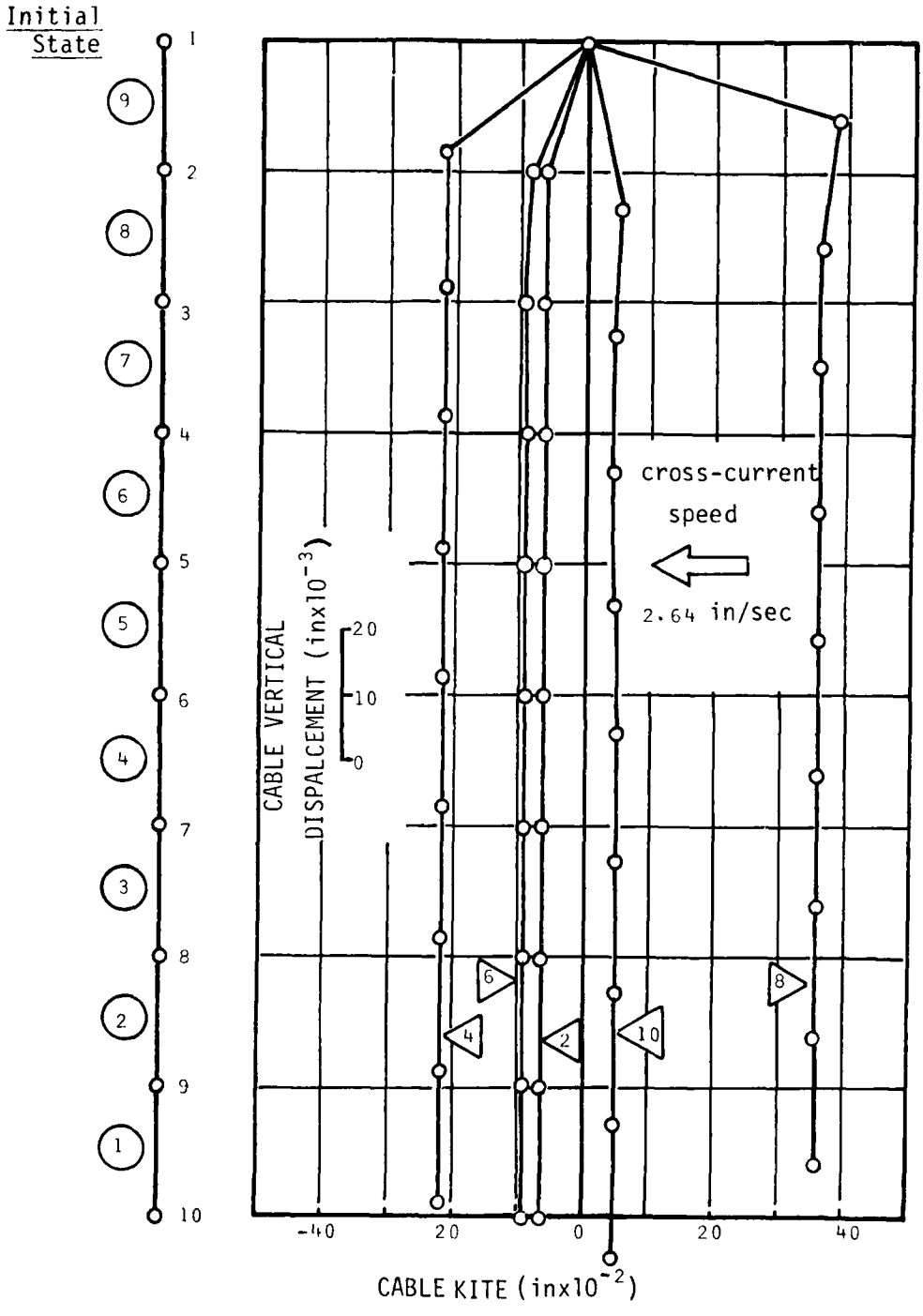

Figure 3.10b
Cable Nodal Relative Positions Orthogonal to the Plane of the Tow (the y, z Plane)

effects then swing the cable back, in opposition to the cross-current (steps 6 through 8). By integration step 10 the cycle is nearly complete, with the cable approaching the plane of the tow and moving with the cross-current. Note that the scales used to plot the node point displacements vary: inches times 10^{-2} for the x- and y-displacements, and "inches x 10^{-3}" for the z-displacements (vertical).

In Figure 3.11 we plot the time history of the average angle of attack along the cable. That the average angle of attack is a reasonable indicator of local behavior is shown by Figure 3.12. The twist of the cable is only marginally less, near the cable's attachment point, than at the free end. The cross-current of 2.64 in/sec. corresponds to an initial angle of attack of 0.573° with respect to the resultant flow. Twisting, induced by the aft location of the hydrodynamic center, with respect to the shear center, causes the cable's angle of attack to vary from the initial (0.573°) to -1.45° (at step 6), then back to 2.16° at step 8, and to 4.72° at step 10. This oscillation in the torsional displacement of the cable contributes to the oscillatory kiting (transverse motion). Moreover, even from the limited duration of these sample computations, it is clear that both the magnitude of the kiting displacement, and the angle of attack, are growing, even though the hydrodynamic center's position -- aft of the shear center -- gives a "statically stable" configuration.

We note once again that the physical parameters of the cable, analyzed above, are not representative of operational cable systems. This sample cable has a very high stiffness-to-length ratio, compared to an operational system. Accordingly, the frequencies and the magnitudes of the oscillations, exhibited, are not representative of operational cables. The complete analysis of an operational system could not be performed during the present developmental effort due to limitations on the computer budget.

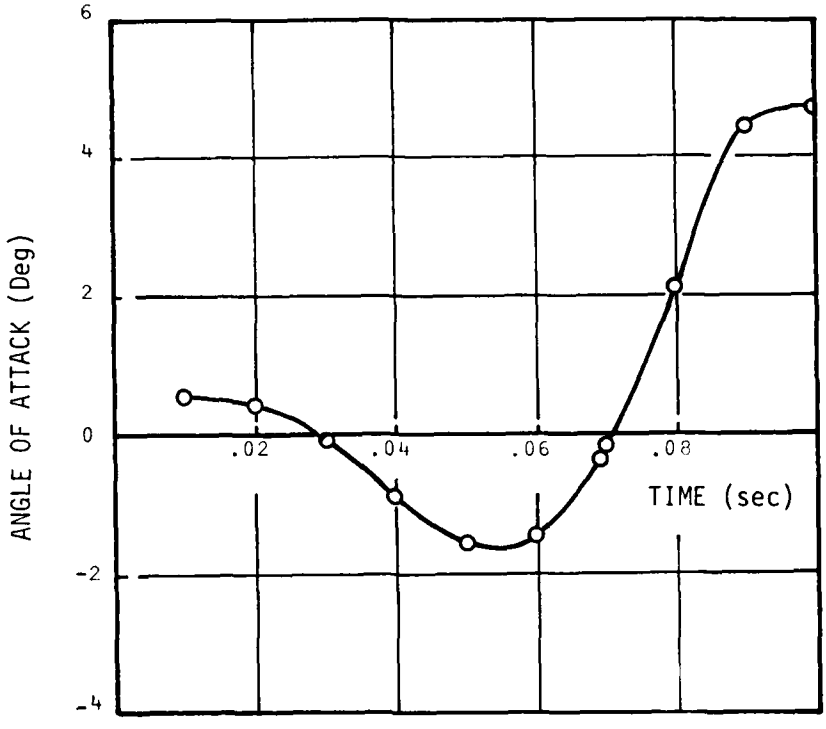

Figure 3.11 Average Angle of Attack Along the Cable

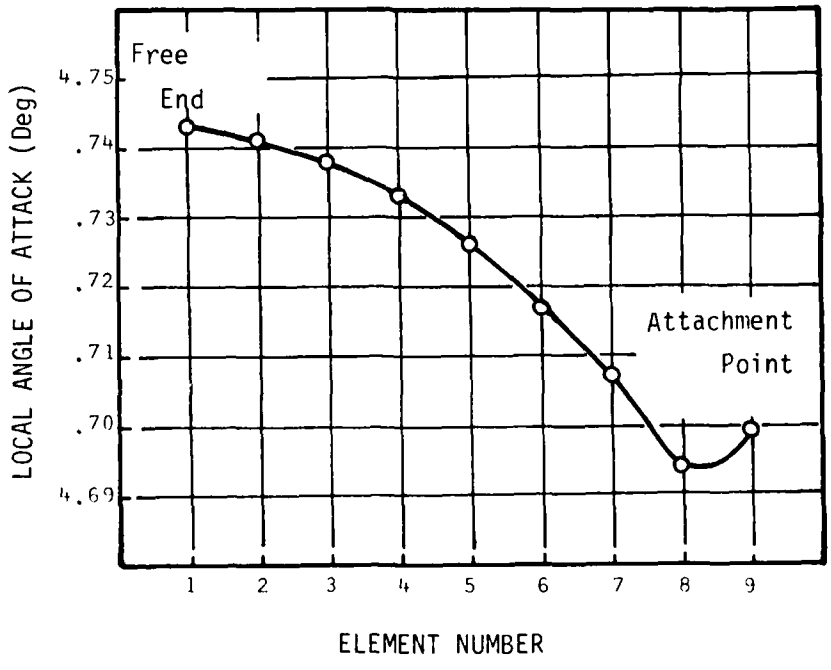

Figure 3.12 Variation in Local Angle of Attack Along the Cable

4.0 CONCLUSIONS AND RECOMMENDATIONS

The initial phases in the development of a computational program, to be used for studying faired, flexible towing cables, has been completed. In the first phase of this task effort, the chordwise deformations, produced on a flexible fairing profile, in a steady, two-dimensional viscous flow, were obtained using the software module HYDROSAP. This is now an operational system which can be used on a production basis to describe the deformations of flexible fairings under hydrodynamic loadings.

In this document the mathematical and physical foundations upon which the HYDROSAP software is based were summarized. In addition, the capabilities of the system were illustrated through the presentation of typical results acquired from its application to several model cable profiles. Even though it was not emphasized here, it should be noted that this program is a fully developed tool for analysis; developed to the extent that it includes highly automated input generator schemes which make it particularly attractive to the analyst-user. In this regard the user is relieved of the troublesome task of building lengthy and complicated input files. Only a minimum of control and descriptive input information needs to be provided in order to run this program.

During the present task significant steps were made toward the completion of a second phase in this program's development effort. Extensions to the two-dimensional computational capabilities, moving toward a full three-dimensional capability, have been embodied -- in preliminary form -- into two additional computer programs, SHCENT and TOWLINE.

As we noted in section 3.0, the three-dimensional, dynamic behavior of a faired cable system, which is modelled in TOWLINE, uses a small strain, large displacement incremental finite element algorithm. For this model, the traditional twelve degree of freedom beam element, of linear structural analysis, has been adapted to the present incremental formulation. Of course, the use of this beam element, to discretize the three-dimensional equations of motion for the cable, requires a knowledge of certain of the mechanical properties (bending and torsional rigid-

ities; shear center location) for the cable's cross-sections. Necessarily, the mechanical properties of heterogeneous, streamlined cross-section profiles, used to describe faired cables, must themselves be computed. We have discussed in this document how the SHCENT program performs that function. Although it is not yet as "user-friendly" as the HYDROSAP module, SHCENT, too, is available for production use.

Even though the TOWLINE program, itself, is operational -- as we have discussed in section 3.0 above -- it is not yet ready for computational production work. First, its input requirements are rather lengthy and cumbersome. No effort has been expended in giving it an automated "user-friendly" input capability. Second, we have found, through an extensive series of check runs, several undesirable performance characteristics which would detract from its use in the eyes of a routine production user.

Due to the combination of an extreme slenderness ratio (span/chord), as is typical of operational towline systems, and the use of an incremental dynamic solution technique, in following the towline to a desired equilibrium state, we have found that the TOWLINE algorithm demands inordinately small time steps. These small time steps are necessary to follow the complicated high-frequency dynamic responses which are apparently exhibited by these cable systems. High frequency oscillations, in addition to cable "whipping", were observed in several of the sample computational runs. Since the required integration time step is of the order of micro-seconds, it is prohibitively expensive to follow a motion for a physically meaningful duration (for several minutes, say). Realistically, the time propagation of numerical errors, inherent to any computational algorithm, would be of serious concern for any run of such magnitude.

Based on our experience with the current version of TOWLINE, then, we recommend that serious attention be given to the development of a non-linear cable finite element. Any such new element formulation would be tailored to the modelling of the structural response, for structural members -- such as cables -- with very high slenderness ratios. However,

unlike existing cable elements which, at most, are capable of undergoing axial extensions, our proposed cable element would also resist both bending and torsion. This new cable element formulation should, of course, not be based on simple models from the linearized theory of strength of materials, but must, instead, incorporate the more recent advances in thin rod theories [19, 20, 21].

Therefore, a general recommendation, based on results acquired from this work, is that the presently used (cable finite element) model should be replaced by a more representative one. With such a properly designed element it is anticipated that many of the present system's computational difficulties will be overcome. It is expected that when this new element model is introduced into (say) the TOWLINE program, it will provide an efficient and useful tool for engineering design and analysis. Concurrent with the development of this new finite element, it is also recommended that the present computational efforts be continued to their intended conclusion. Then, the completed system can and should be placed into operation as a design and study tool for high-speed, flexible towline systems.

5.0 REFERENCES

[1] Eades, J. B. and V. Majer, "Program Development to Study Faired Towlines", ONR-CR198-003-1, 1979.

[2] Brune, G. W. and J. W. Manke, "An Improved Version of the NASA/ Lockheed Multi-Element Airfoil Analysis Computer Program". NASA CR-145323, March 1978.

[3] Morgan, H. L., Jr., "A Computer Program for the Analysis of Multi-Element Airfoils in Two-Dimensional Subsonic, Viscous Flow". Aerodynamic Analyses Requiring Advanced Computers Conference. NASA/Langley Research Center, Hampton, Virginia, March 1975.

[4] Stevens, W. A., S. H. Goradia, and J. A. Braden, "Mathematical Model for Two-Dimensional Multi-Component Airfoils in Viscous Flow". NASA CR-1843, July 1971.

[5] Oeller, H. J., "Die inkompressible Potentialstromung in der ebenen Gitterstufe (Incompressible Potential Flow in Two-Dimensional Cascades)". Wissenschaftliche Gessellschaft fur Luft-und Raumfahrt E. V., pp. 349-353, Jahrbuch 1962 (In German, not translated).

[6] Dvorak, F. and B. Maskew, "The Prediction of $C_{\ell max}$ Using a Separated Flow Model", Proceedings of the 33rd AHS Meeting, 1977 (Paper No. 77.33.01). Also, Journal American Helicopter Society, April 1978.

[7] Cohen, C. B. and E. Reshotko, "The Compressible Laminar Boundary Layer with Heat Transfer and Arbitrary Pressure Gradient", NASA TND-1294, 1956.

[8] Schlichting, H., BOUNDARY LAYER THEORY. Sixth Ed., McGraw-Hill, New York, 1968.

[9] Truckenbrodt, E., "Ein Quadraturuerfahren zur Berchnung der laminaren und turbul.nten Reibungsschift bei ebener und rotationssymmetrischer Stromung", Ing. Arch., vol. 20, pp. 221-228, 1952 (NASA TM-1379, 1955).

[10] Squire, H. B. and B. A. Young, "The Calculation of the Profile Drag of Airfoils", RAE Report R&M No. 1838, November 1937.

[11] Bathe, K. J., H. Ozdemir, and E. L. Wilson, "Static and Dynamic Geometric and Material Nonlinear Analysis", Report No. UC SESM 74-4, Structural Engineering Laboratory, Department of Civil Engineering, University of California, Berkeley, California, 1974.

[12] Bathe, K. J., E. L. Wilson, and R. H. Iding, "NONSAP: A Structural Analysis Program for Static and Dynamic Response of Nonlinear Systems", Report No. UC SESM 74-3, Structural Engineering Laboratory, Department of Civil Engineering, University of California, Berkeley, California, 1974.

[13] Oden, J. T., FINITE ELEMENTS OF NONLINEAR CONTINUUA, McGraw-Hill, 1972.

[14] Zienkiewicz, O. C., THE FINITE ELEMENT METHOD IN ENGINEERING SCIENCE, McGraw-Hill, London, 1971.

[15] Baumgartner, E. M. E., "Finite Element Solution of Torsional Stiffness and Shear Center for Sections of Arbitrary Shape and Composition", NTIS N78-32494, November 1977.

[16] Rivello, R. M., THEORY AND ANALYSIS OF FLIGHT STRUCTURES, McGraw-Hill, New York, 1969.

[17] [illegible]z, F., "Uber den Schubmittelpunkt in einen durch eine [illegible]st gebogenen Balken", Z. Angew, Math. Mech. 15, [illegible], 1935.

[18] Yeung, K. S. and R. E. Welch, :"Automobiles under Crash Loading", IIT Research Institute, October 1977.

[19] Antman, S. S., "Ordinary Differential Equations of Non-Linear Elasticity I: Foundations of the Theories of Non-Linearly Elastic Rods and Shells", Archive for Rational Mechanics and Analysis, V. 61, no. 4, pp. 307-351, 1976.

[20] Green, A. E. and N. Laws, "A General Theory of Rods", Proceedings of the Royal Society (London) A293, pp. 145-155, 1966.

[21] Antman, S. S. and J. E. Osborn, "The Principle of Virtual Work and Integral Laws of Motion", TR-78-38, University of Maryland, 1978.

APPENDIX A Hydrosap Computer Program

A.1 Program Description

The Hydrosap computer program computes the deformed configuration of a two-dimensional "flexible" fairing at angle of attack in a steady viscous fluid flow. The program consists of three segments: HYDRO, for the "fluids" computations; NONSAP, for the mechanical response computations, and DRIVER, an executive sub-program which initializes and controls the computations. The NONSAP segment consists of routines selected from the University of California Non-linear Structural Analysis Program while the HYDRO segment is an adaptation of the NASA Multi-component Two-dimensional Viscous Airfoil Program. Since we have discussed the details of HYDRO and NONSAP operations elsewhere [1], and since the user "sees" only the front-end executive, DRIVER, we discuss in this Appendix only the DRIVER input deck.

A.2 DRIVER Input Deck

The HYDROSAP input cards are identified with Tape 5 (usually the system input stream). The input stream consists of six distinct card groups, not all of which are present in a single run. Only the first two card groups must be present; the presence or absence of the other four groups is determined from values assigned by the user to the NONSAP control variables SHRTIN, HYDSIM, SAPSIM, and N. All of the control variables are defined below. The input stream groups are as follows:

CARD GROUP 1 Title Card

Card 1.1 Title of Run
I
Up to an 80 character title for the run.
(This card must appear.)

CARD GROUP 2 Control Variables

Card 2.1 $DRV
12
Header card for NAMELIST /DRV/; signals the beginning of the control input. (This card must appear.)

Definitions of the DRV NAMELIST variables are as follows:

A.2.1 Control Variable Definitions

The HYDROSAP Control Variables (Card Group 2 of the HYDROSAP Input) fall into two groups: logical variables and arithmetic variables. The logical variables are true/false switches used to activate the various program options. The arithmetic variables are used to set values for the integer and real variables which control the flow of computations (examples are: iteration counters, output units, mesh fineness, and convergence tolerance), or define the physical parameters of the problem under study (such as flow conditions and material properties). Detail definitions of the control variables are as follows:

VARIABLE	TYPE	DEFAULT		INTERPRETATION
CHKPNT (CHeckPoiNT)	LOGICAL	.FALSE.	=.TRUE.	Produce checkpoint tape (FT14FØØ1)
			=.FALSE.	Checkpointing disabled.
CORE	LOGICAL	.FALSE.	=.TRUE.	Fairing has a cable (core) material
			=.FALSE.	No distinct cable (core) present
			(SHRTIN=.TRUE. only)	
DEBUG	LOGICAL	.FALSE.	=.TRUE.	Special print in LOADER: HYDRO and NONSAP output provided at each HS iteration (iteration = outer loop)
			=.FALSE.	HS print produced at start of run only. No debug output.

VARIABLE	TYPE	DEFAULT		INTERPRETATION
ECHO	LOGICAL	.TRUE.	=.TRUE.	Echo of HYDRO and NONSAP input decks produced.
			=.FALSE.	Suppress "echo" of files.
HYDSIM (HYDro SIMulation)	LOGICAL	.FALSE.	=.TRUE.	Program operates in the HYDRO simulation mode (SAPSIM must be .FALSE.)
			=.FALSE.	Signifies a request for the full HYDROSAP run; or NONSAP simulation, depending on the value assigned to SAPSIM.
POST	LOGICAL	.FALSE.	=.TRUE.	The Graphics Post-processor output is directed to Unit 88.
			=.FALSE.	No operation requested.
RESTRT	LOGICAL	.FALSE.	=.TRUE.	Read checkpoint tape and restart at time TSTART
			=.FALSE.	Restart disabled.
SAPSIM	LOGICAL	.FALSE.	=.TRUE.	Program is to operate in NONSAP simulation mode (HYDSIM must be set to .FALSE.)
			=.FALSE.	Full HYDROSAP run; or HYDRO simulation, depending upon value assigned to HYDSIM.
SHRTIN (SHoRT form INput)	LOGICAL	.TRUE.	=.TRUE.	Signifies the short form input. An automatic input file generation occurs (for foil geometry and state).
			=.FALSE.	HYDRO and NONSAP input decks, separated by 999999999, must follow $DRV-$END on SYSIN file.

VARIABLE	TYPE	DEFAULT	INTERPRETATION
SKIN	LOGICAL	.FALSE.	=.TRUE. Denotes the fairing cross-section has a skin attached. =.FALSE. No skin member is presumed.
TAIL	LOGICAL	.TRUE.	=.TRUE. The fairing has a fairing "tail" member. =.FALSE. No fairing tail is assumed (CORE must be set to .TRUE. in this case).
TPRINT (Terminal PRINT)	LOGICAL	.TRUE.	=.TRUE. Terminal summary output (error msgs. and job flow) =.FALSE. No terminal print.
INTORD (INTerpolation ORDer)	INTEGER	3	Denotes the interpolation order for the pressure distribution conversion from the HYDRO surface to the NONSAP surface.
INTORX (INTerpolation ORder X)	INTEGER	1	Interpolation order to be assigned for the displacement conversion from the NONSAP surface to the HYDRO surface.
IPANEL	INTEGER	2	IPANEL is equivalent to HYDRO control variable IOP.
IPAPER	INTEGER	6	Unit number assigned to the HYDROSAP DRIVER module output.
IPRINT	INTEGER	=NSTEPS	Denotes the NONSAP print frequency within HYDROSAP ITERATION #1.
ISMTH	INTEGER	0	ISMTH is equivalent to HYDRO control variable ISMO.
ITRSWT (ITeRation SWiTch)	INTEGER	8	The number of HYDROSAP iterations using HYDRO potential flow solution mode only.
IWRTØ	INTEGER	6	Denotes the NONSAP output UNIT.

VARIABLE	TYPE	DEFAULT	INTERPRETATION
IWRT1	INTEGER	6	Denotes the HYDRO output unit.
LOOPMX (LOOPMaXimum)	INTEGER	1	Signifies the maximum number of HYDROSAP iterations (outer loops) allowed.
MESHC (MESHChordwise)	INTEGER	1	Denotes the number of chordwise interior stations used to generate the finite element mesh, when SHRTIN is set to .TRUE.
MESHT (MESHThickness-wise)	INTEGER	1	Denotes the number of lateral interior stations used to generate the finite element mesh when SHRTIN is set to .TRUE.
N	INTEGER	Ø	N>Ø Signifies the number of upper surface coordinate pairs to be input through NAMELIST $FAIRNG-$END, following NAMELIST $DRV-$END, on SYSIN. N=Ø Means no fairing profile is input. N<Ø A pointer for profile library routine |N|. Thus, N= -2 reads profile points from subroutine FOILØ2. (Applicable when SHRTIN set to .TRUE., only.)
NSTEPS	INTEGER	2Ø	Denotes the number of (quasi-static) load steps to be used in applying the field pressure load to a fairing, in NONSAP, during HYDROSAP iteration #1.

Note: NSTEPS should be increased when the message "OUT-OF-BALANCE LOADS EXCEED INCREMENTAL LOADS" is obtained.

ALPHA	REAL*8	Ø.DØ	Angle of attack (deg.)
ECORE	REAL*8	1.DØ6	Young's modulus for the core material (psi).
ESKIN	REAL*8	1.DØ4	Young's modulus for the skin material (psi).

VARIABLE	TYPE	DEFAULT	INTERPRETATION
ETAIL	REAL*8	1.DØ4	Young's modulus for the fairing tail material (psi).
PCORE	REAL*8	.3	Poisson ratio for the core, skin, and tail, respectively.
PSKIN		Ø	
PTAIL		.3	
PZERO	REAL*8	14.7DØ	Static pressure loading (psi).
RHO	REAL*8	2.DØ	H_2O density (slugs/ft^3).
TOL	REAL*8	$1 \times 1Ø^{-2}$	Denotes the HYDROSAP convergence tolerance level. Convergence is achieved when rms displacement increment <(rms displacement) * TOL.
TSKIN	REAL*8	.ØØ5	Skin thickness (inches) (applies only if SKIN is set to .TRUE.).
TSTART (Time of reSTART)	LOGICAL	Ø.DØ	Applies only when RESTRT= .TRUE. HYDROSAP will restart at checkpoint for time TSTART.
VFRSTR	REAL*8	22.DØ	Freestream velocity (ft/sec)
VFRSTR	REAL*8	22.DØ	Free stream velocity (fps).
Y1CORE	REAL*8	Ø.DØ	Chordwise location of the core starting point.
Y2CORE	REAL*8	Ø.DØ	Chordwise location of the core ending point.

Card 2.2 SHRTIN=T,···
123
⋮ Input as many cards as required to override default control variable values.

Card 2.n

Card 2.n+1 $END
12
End card for NAMELIST /DRV/; signals the termination of the namelist string. (This card must appear.)

CARD GROUP 3 Cable Fairing Profile Namelist (optional)
Card Group 3 is present only if SHRTIN=T and N>0 in NAMELIST /DRV/.

Card 3.1 $FAIRNG
12
Header card for NAMELIST /FAIRNG/.

Card 3.2 XX(1)=···,XX(N)=···,
123
⋮

Card 3.m ZZ(1)=···,ZZ(N)=···,
123
{(XX(I),ZZ(I)), I=1,···N} are the profile coordinates, in inches, for the upper surface of the symmetric cable fairing to be modeled. N is set in NAMELIST /DRV/.

Card 5.m+1 $END
12
End card for NAMELIST /FAIRNG/.

CARD GROUP 4 HYDRO Input Deck (optional)
Card Group 4 is present only if SHRTIN=F and SAPSIM=F in NAMELIST /DRV/.

Card 4.1 First card of HYDRO input deck

⋮ ⋮ } see section 3.3

Card 4.p Last card of HYDRO input deck.

CARD GROUP 5		Spacer
	Card 5.1	99999999 12345678 A spacer card to be inserted between HYDRO and NONSAP input decks. (This card must be present whenever SHRTIN=F.)
CARD GROUP 6		NONSAP Input Deck (optional) Card Group 6 is present only if SHRTIN=F and HYDSIM=F in NAMELIST /DRV/.
	Card 6.1	First card of the NONSAP input deck.
	⋮	⋮ } see section 4.3
	Card 6.q	Last card of the NONSAP input deck.

APPENDIX B. SHCENT Computer Program

B.1 Program Description

The SHear CENTer (SHCENT) program computes the St. Venant warping function for an arbitrarily shaped, heterogeneous, orthotropic cross-section. The SHCENT program was adapted from a code developed by E. Baumgartner [15]. Using the warping function, the program computes the section's torsional rigidity and the coordinates of its shear center. Incidental to the warping function computations, the program also computes the bending rigidities of the section, the modulus weighted area for the section, and the location of the modulus weighted centroid. Written in FORTRAN, the program accepts, as input, the topology of Ω (the section shape) and its triangulation, as well as the material constants for each element of the triangulation.

B.2 Problem Size Limitations

The current double precision version of the program runs in 224k bytes of core on an IBM system 360/91. With this program size, the triangulation of Ω is limited to:

- maximum number of triangular elements - 140
- maximum number of nodal points - 150
- maximum number of different materials comprising the cross-section - 20
- maximum semi-bandwidth for the global stiffness matrix - 100.

All significant variables are passed among the various subroutines of SHCENT via blank common. The problem size limitations (above) are trivially eased by altering the dimensions of the variables in blank common.

B.3 SHCENT Input Deck

Program SHCENT reads input from FORTRAN Unit 5 using list-directed (free-field) format. The programmer may comment his input deck by placing an asterisk (*) in the first column of the comment record. A rudimentary mesh generating option is available for automatically computing model coordinates and element definitions for "regular" meshes. For this, element nodes must be "numbered" counterclockwise.

A description of the input deck follows:

Title Card

Card 1: TITLE

TITLE - Any 80 characters alphanumeric to be used as the title for a run

Control Card

Card 2: NODNO, NGMAT, NGRELM, NGRNOD, NECHO

NODNO - Total number of nodes

NGMAT - Number of material property vectors to be read

NGRELM - Number of element definition groups to be read

NGRNOD - Number of node point definition groups to be read

NECHO - Input echo flag

= 0, No echo of input

= 1, Echo input

Material Property Cards

Cards 3: K, (GMAT(k,j),j=1,4) (input NGMAT cards)

GMAT(k,1) - G_{xz} , xz shear constant

GMAT(k,2) - G_{yz} , yz shear constant

GMAT(k,3) - E_z , Young's modulus orthogonal to the cross-section

GMAT(k,4) - α , angle (degrees) between material axes and input coordinate system

Element Definition Cards

Cards 4: NGR, IL, ILA, IS, IA, JS, JA, KS, KA, NMAT

- NGR - Number of elements to be defined by this card
- IL - Element number of first element in the group
- ILA - Increment by which IL is to be increased (decreased for ILA<0) for each additional element defined in this group
- IS - Global node number of element (local node) number 1
- IA - Node number increment for IS (cf. ILA)
- JS - Global node number of element (local node) number 2
- JA - Node number increment for JS
- KS - Global node number of element (local node) number 3
- KA - Node number increment for KS
- NMAT - Material property vector to be associated with this element (cf. K of CARDS 3)

Node Point Definition Cards

CARDS 5: NGR, J, JA, Y(J), DY, Z(J), DZ

- NGR - Number of nodes to be defined by this card
- J - Node number of first node in this group
- JA - Increment by which J is to be increased (or decreased, for JA<0) for each additional node defined in this group

Y(J)Z(J)-local or global coordinates of node J

DY,DZ - coordinate increments by which Y(J) and Z(J), respectively are to be increased for each additional node defined in this group

End of Data Card

Card 6: -999 , in columns 1-4.

AD-A083 940 BUSINESS AND TECHNOLOGICAL SYSTEMS INC SEABROOK MD F/G 13/10
PROGRAM DEVELOPMENT TO STUDY FAIRED TOWLINES.(U)
FEB 80 J B EADES, V MAJER N00014-78-C-0410
UNCLASSIFIED BTS-IR-80-102 ONR-CR298-003-2F NL

2 OF 2
AD
A083940

END
DATE FILMED
4-80
DTIC

APPENDIX C TOWLINE Computer program

C.1 Program Description

The TOWLINE program computes the three-dimensional dynamic (or quasi-static) response of a faired towing cable under the assumption that the cable, while undergoing large displacements, sustains only small strains. A standard three-dimensional beam element formulation is used to discretize the cable.

Written in FORTRAN, the program accepts as input an initial configuration of the cable and the mechanical and hydrodynamic properties of the elements into which the cable has been subdivided. Up to ten different beam cross-section types can be accommodated. The user may specify time-dependent external forcing functions, in tabular format, or supply a user-written subroutine (FORCE) to define the forcing functions explicitly. A checkpoint-restart capability makes possible the resumption of computations from a previous run.

C.2 Problem Size Limitations

The current double-precision version of the program runs in 498K bytes of core on an IBM System 360/91 system. With this program size the discretization of the cable is limited to 100 nodes (99 elements).

C.3 TOWLINE Input Deck

Program TOWLINE accepts input from FORTRAN Unit 5 using formatted reads. A description of the input variables and card formats follows:

CARD 1: KEY, TITLE (19) FORMAT (A1, 19A4)

KEY - decision flag for integration procedure
= E, explicit
= I, implicit

TITLE - 76 character titles for the run

CARD 2: NNODE, NELE, NUMMAT, FORMAT (6I5, E10.6,4I5)
NUMDIS, MXSTEP, NDGREE,
DELT, NCOORD, NSECT, NFUN,
IAERO

NNODE - number of structural nodes (max 100)
NELE - number of elements (max 100)
NUMMAT - number of different material models
NUMDIS - number of nodes at which displacement, velocity, or force are to be specified, as functions of time
MXSTEP - maximum number of time steps
NDGLEE - number of degrees of freedom per node (=6 for current version)
DELT - time step size (secs)
NCOORD - number of beam cross-section pointer nodes
NSECT - number of different beam cross-section types
NFUN - number of different time-dependent functions (max = 9)
IAERO - decision flag for hydrodynamic loads
= 0, no hydrodynamic loads
= 1, include hydrodynamic loads

CARD 3: RHO,V(3)

RHO - fluid density
V - fluid velocity vector, with respect to cable, in global (x,y,z) coordinates (x-z plane represents plane of tow; z axis along gravity vector)

NOTE: OMIT CARD 3 IF IAELO = 0.

CARD 4: KONTRL (10) FORMAT (10I5)

KONTRL (1) - stiffness matrix update frequency
(2) - not used
(3) - not used
(4) - not used
(5) - βx1000; Newmark - beta
(6) - not used
(7) - not used
(8) - checkpoint/restart control
= 0, no operation
= n, checkpoint every n steps on unit 25
= -n, restart and then make checkpoint every n steps
(9) - restart checkpoint number
(10) - time history frequency
< 0, no operation
= n, make time history of motion on unit 22 every n steps.

CARD 5.1: MTYPE FORMAT (I5)

MTYPE - material model number

CARD 5.2 & 5.3 E(16) FORMAT (8F10.0)

E(1) - material density
E(2) - modulus of elasticity
E(3)-E(6)- not used
E(7) - Poisson's ratio
E(8)-E(16)-not used

NOTE: REPEAT CARD GROUP 5 NUMMAT TIMES

CARD 6.1: NSEG, KLOS, IYY, IZZ, J FORMAT (2I5,3F10.0)

NSEG - number of plate sections in beam cross-sections (set NSEG=1 if KLOS=2)

KLOS - cross-section type
= 0, thin walled closed section
= 1, thin walled open section
= 2, full cross-section with user specified cross-section

IYY - user-supplied cross-section moments of inertia
IZZ about local y and z axes, respectively, of the section

J - user-supplied cross-section torsion constant

CARDS 6.2: Y(I), Z(I), T(I), I=1,KLOS+NSEG FORMAT (3F10.4)

Y(I) - cross-section coordinate of point at beginning of
Z(I) plate segment I (cf. Figure c.1 below)

T(I) - thickness of cross-section plate segment I

NOTE: (1) If KLOSO=2, then Y(3),Z(3) are the coordinates of the modulus-weighted centroid of the section with respect to the section coordinate system (origin at the section's shear center). T(2) and T(3) are ignored in this case.

(2) Input NSEG+KLOS cards in group 6.2

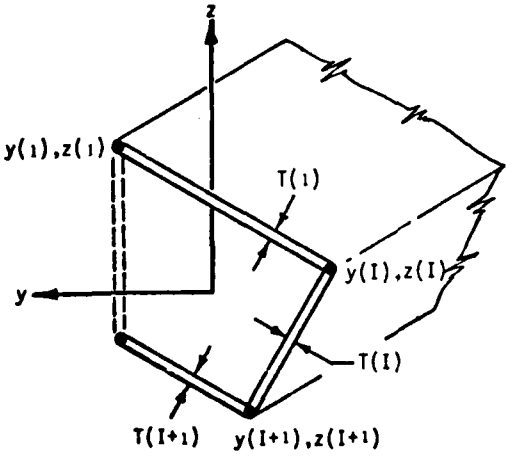

Figure c.1a Thin Wall Beam Cross Section

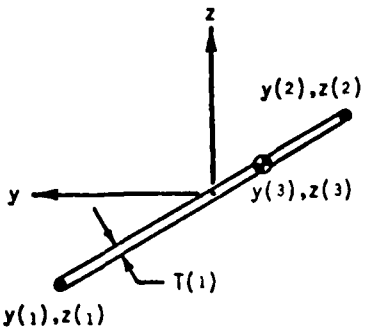

Figure c.1b Full Beam Cross-section

DISTRIBUTION LIST

Office of Naval Research
800 N. Quincy St.
Arlington, VA 22217
- ONR 211 — 4
- ONR 222 — 1
- ONR 438 — 1

Office of Naval Research Branch Office
1030 E. Green St.
Pasadena, CA 91106 — 1

Office of Naval Research Branch Office
Bldg. 114 Section D
666 Summer St.
Boston, MA 02210 — 1

Office of Naval Research Branch Office
536 South Clark St.
Chicago, IL 60605 — 1

Naval Research Laboratory
Washington, DC 20375
- Code 2627 — 1
- Code 2629 — 1
- Code 8441 (Dr. R. J. Hansen) — 1

Defense Technical Information Center
Bldg. 5 Cameron Station
Alexandria, VA 22314 — 12

Naval Sea Systems Command
Washington, DC 20362
- Code 03512 (Dr. T. Peirce) — 1

David Taylor Naval Ship Research and Development Center
Bethesda, MD 20084
- Main Liabrary, Code 522.1 — 1
- Code 1548 (Dr. P. Rispin) — 1
- Code 1843 (Ms. J. Schot) — 1

Naval Surface Weapons Center
White Oak Laboratory
Silver Spring, MD 20910
- WA-41 (Mr. W. J. Yanta) — 1

California State University - Long Beach
Mechanical Engineering Dept.
Long Beach, CA 90840
- Prof. T. Cebeci — 1

U. S. Naval Postgraduate School
Monterey, CA 93940
- Dept. of Aeronautics (Code 57) — 1
- Library — 1

Superintendent
U. S. Naval Academy
Annapolis, MD 21402 — 1

Stevens Institute of Technology
Davidson Laboratory
Hoboken, NJ 07030
- Dr. T. R. Goodman — 1

California Institute of Technology
Graduate Aeronautical Labs.
Pasadena, CA 91109
- Prof. H. W. Liepman — 1

Naval Coastal System Lab.
Panama City, FL 32401
- Library — 1
- Code 794 (Dr. D. Humphreys) — 1

Vought Corporation
Advanced Technology Center, Inc.
P. O. Box 6144
Dallas, TX 75222
- Dr. C. S. Wells, Jr. — 1

Dynamics Technology, Inc.
3838 Carson St., Suite 10
Torrance, CA 90503
- Dr. D. Ko — 1

Analytical Methods, Inc.
100 - 116th Ave. S.E.
Bellevue, WA 98004
- Dr. F. Dvorak — 1

Massachusetts Institute of Technology
Dept. of Ocean Engineering
Cambridge, MA 02139
- Prof. M. A. Abkowitz — 1

University of Michigan
Dept. of Naval Architecture & Marine Engineering
Ann Arbor, MI 48109
- Prof. T. Francis Ogilvie — 1

National Science Foundation
Engineering Division
1800 G. St. NW
Washington, DC 20006 — 1